Climate friction and the Earth's obliquity

B. Levrard

Geophys. J. Int. (2003) **154,** 970–990

Climate friction and the Earth's obliquity

B. Levrard and J. Laskar

Astronomie et Systèmes Dynamiques, IMCCE, Observatoire de Paris, 77*, Avenue Denfert-rochereau* 75014 *Paris, France. E-mail: blevrard@imcce.fr*

Accepted 2003 April 30. Received 2003 April 7; in original form 2002 October 21

SUMMARY

We have revisited the climate friction scenario during the Earth's major glacial episodes of the last 800 Myr: the Late Pliocene-Pleistocene (∼0–3 Ma), the Permo-Carboniferous (∼260–340 Ma) and the Neoproterozoic (∼750 ± 200 Ma). In response to periodic variations in the obliquity, the redistribution of ice/water mass and the isostatic adjustment to the surface loading affect the dynamical ellipticity of the Earth. Delayed responses in the mass redistribution may introduce a secular term in the obliquity evolution, a phenomenon called 'climate friction'. We analyse the obliquity–oblateness feedback using non-linear response of ice sheets to insolation forcing and layered models with Maxwell viscoelastic rheology. Since the onset of the Northern Hemisphere glaciation (∼3 Ma), we predict an average drift of only ∼0.01 deg Myr^{-1} modulated by the main ∼1.2 Myr modulating obliquity period. This value is well reproduced when high-resolution oxygen-isotope records are used to constrain the ice load history. For earlier glaciations, we find that the climate friction effect is not proportional to the amplitude of the ice-age load, as it was previously assumed. A possible increase in the non-linear response of ice sheets to insolation forcing and latitudinal changes in this forcing may strongly limit the contribution of the obliquity variations to glacial variability, and thereby the climate friction amplitude. The low-latitude glaciations of the Sturtian glacial interval (*ca* 700–750 Ma) have probably no influence on the obliquity, while we predict a maximal possible absolute change of ∼2° for the Varanger interval (*ca* 570–620 Ma). We show that this mechanism cannot thus explain a substantial and rapid decrease in obliquity (of ∼30°) as previously suggested by D.M. Williams *et al.* (1998) to support the high obliquity scenario of G.E. Williams (1993). Overall, we find that climate friction cannot have changed the Earth's obliquity by more than 3–4° over the last 800 Myr.

Key words: inertia (moments of), Neoproterozoic, obliquity, Palaeoclimatology, Pleistocene, Rheology.

1 INTRODUCTION

The obliquity of the Earth is one of the main palaeoclimatic quantities. It influences both the seasonal contrast in each hemisphere, and the latitudinal distribution of the incident solar radiation. Quasi-periodic fluctuations of the obliquity, conjugated to the long-term variations of the Earth's orbital parameters (eccentricity, climatic precession) that control the amount of the incident insolation, are largely implicated in the extreme changes of climate of the Late Pliocene–Pleistocene period. Analyses of isotopic $\delta^{18}O$ ratio extracted from foraminifera shells of deep-sea marine sediments, largely demonstrate that global ice volume varies with the same periodicities as those of the astronomical forcing, as originally proposed by Milankovitch. In particular, the succession of marked glaciation–deglaciation episodes that have occurred since the onset of the glaciation in the Northern Hemisphere (about 3 Ma) shows a large dominance of the main 41 kyr obliquity cycle (Ruddiman *et al.* 1989; Raymo *et al.* 1989). Although the glacial variability has shifted to a dominant 100 kyr cycle at the well-known Mid-Pleistocene transition (∼0.8 Ma), it still contains a significant power in the obliquity band (Hays *et al.* 1976; Imbrie *et al.* 1984). One dissipative mechanism which can affect the Earth's mean obliquity is called 'climate friction', acting through a positive feedback between glaciations and the obliquity motion. The oscillations between glacial and interglacial conditions, partly caused by obliquity variations, are characterized by a transfer of large amounts of water between ice sheets and oceans that alter the shape of the Earth and cause variations in its dynamical ellipticity. Although a significant fraction of the surface loading tends to be compensated by the viscous flow within the interior of the Earth, the fluctuations of the dynamic ellipticity still contain a small obliquity-induced periodic term which acts as an external forcing function on the Earth's precession motion, and hence on the obliquity oscillations, analogous to a resonant excitation. An important consequence is that a secular drift in the mean obliquity may result via delayed responses in the redistribution of mass both on and within the Earth. The existence of two delayed

and dissipative processes associated on one hand to the ice sheet response to obliquity variations, and on the other hand to the mantle viscous adjustment to surface loading, can lead to either an increase or a decrease in the obliquity, depending on the magnitude of each phase lag.

Several previous analyses have examined this phenomenon, as applied to Mars (Rubincam 1990, 1993, 1999; Spada & Alphonsi 1998; Bills 1999). For the Earth, there have been a number of attempts to estimate its potential impact but the amplitude and the direction of the secular drift are largely controversial. Bills (1994) used a parameterized model with uninterrupted ice ages and estimated that a very large drift, higher than 60° in 100 Myr, was possible. However, it was asserted that net changes of the dynamical ellipticity through a typical ice-age cycle could be of the order of 1 per cent, an upper value estimated only for a rigid Earth, incapable of isostatic adjustment. Rubincam (1995) derived an analytical explanation of the secular obliquity change and described the relaxation process with the simple Darwin model consisting of a uniform sphere with Newtonian rheology. He suggested that the change of Earth's obliquity is probably positive and cannot have been more than 15–35° over the Earth's entire glacial history (∼450 Myr) if all previous ice-ages were similar to Quaternary conditions. This rate was estimated when the periodic change in obliquity is reduced to its main 41 kyr cycle. Ito *et al.* (1995) computed numerical integrations of the feedback loop, using a linear correlation between ice sheet formation and the high-latitude summer insolation, including viscoelastic layered models. Nevertheless, for Quaternary glaciations, they found a computed positive secular obliquity change close to ∼0.05 deg Myr^{-1}, in large disagreement with their theoretical rate (recalculated from their eq. 36) of 0.25 deg Myr^{-1}.

Conversely, D.M. Williams *et al.* (1998) suggested that climate friction could have produced a decrease larger than ∼30° of the Earth's obliquity in less than 100 Myr between ∼600 Ma and 500 Ma near the end of the Neoproterozoic Era. They argued that the complete and periodic waxing and waning of hypothetical huge ice sheets on a permanent South polar supercontinent may have yielded a large relative change of rigid-Earth oblateness close to 2.6 per cent, and a proportional enhancement of the secular drift. In addition, the negative direction could have been caused by an extreme ice sheet response phase lag to obliquity variations close to 225°. However, as in Ito *et al.* (1995), we found a large disagreement between their predicted numerical rate (∼ −0.3 deg Myr^{-1}) and their theoretical estimation close to ∼ −2 deg Myr^{-1} (from their eq. 1). An important consequence of this large obliquity decrease was to provide a natural support of the Proterozoic high obliquity scenario of G.E. Williams (1975, 1993).

The Neoproterozoic Era has recently drawn special attention, as the Earth probably experienced extreme changes in biological activity, geochemical effects and climate regimes during this time (e.g. Knoll & Walter 1992). In particular, many palaeomagnetic data and glacial records display the presence of widespread and severe glaciations on most of the continents (e.g. Crowell 1999; Evans 2000). Recent palaeomagnetic studies have confirmed the presence of paradoxical low-latitude glaciogenic deposits below 20° and at sea level (Schmidt & Williams 1995; Park 1997; Sohl *et al.* 1999)

To account for the widespread and low-latitude glaciations, Williams (1975, 1993) proposed that high obliquity (>54°) has persisted for a large time of Earth's history until ∼600 Ma, which would make equatorial zones colder than polar zones, and cause preferentially low-latitude glaciations as well as related and observed permafrost features, due to marked seasonal changes of temperature. The hypothetical end of glaciations (∼600 Ma) would then have been linked to a large decrease of obliquity by more than 30° in 200 Myr until ∼430 Ma, time when palaeo-tidal data indicate an obliquity close to the present one (Williams 1993). Conversely, early palaeomagnetic studies which suggested the presence of low-latitude glaciations, have led to the concept of a worldwide glacial interval when the world had essentially frozen over (Harland 1964). This hypothesis became the 'Snowball Earth' hypothesis, suggested by the presence of glaciogenic iron deposits (Kirschvink 1992). Large negative carbon isotope anomaly data from carbonate rocks capping Neoproterozoic glacial deposits (Hoffman *et al.* 1998; Hoffman & Shrag 2002) recently gave new support to this theory, leaving the possibility that the Earth's oceans were entirely cut-off from the atmosphere for as much as 10 Myr as a result of a global glaciation.

Here, we present a re-estimation of the secular effect of climate friction that can be reconciled with numerical integrations. We found that both theoretical and numerical analyses of Ito *et al.* (1995) and Williams *et al.* (1998) are not consistent with the initial mechanism proposed by Rubincam (1990, 1995). Once this reconciliation has been made, we investigate in details the properties and the main constraints of the climate friction effect during the recent major glacial episodes of the Earth. The previous studies, limited to Quaternary glaciations, are extended to the onset of the Northern Hemisphere glaciation (∼3 Ma) that encompasses the entire Pleistocene and the Late Pliocene, and corresponds to the more intense episode of the Late Cenozoic glaciation (∼0–35 Ma). Although the Pre-Cenozoic glaciations are still poorly constrained in time and space (e.g. Crowell 1999), we try to give some constraints on the climate friction amplitude during Permo-Carboniferous and Neoproterozoic glacial episodes. In particular, we discuss the effect of non-linearities in the ice volume response to insolation forcing, and of the extension of the ice caps during possible larger glaciations. In particular, we found that the predominantly low-latitude glaciations predicted by G.E. Williams' (1993) high obliquity scenario, cannot affect the Earth's mean obliquity, because their location will minimize the climate friction effect.

Clearly, the issues developed for each glacial period are quite different. The vast array of high-resolution and long benthic δ^{18}O records collected over the last 25 yr provided useful information about the timing and the amplitude of the global ice volume response at Milankovitch frequencies during Cenozoic glaciations. Unfortunately, such accurate data are not available for earlier glaciations. To what extent present observations and associated climatic processes can be used for earlier glaciations is still unclear, but it provides a natural and simple tool for such an investigation.

The remainder of this paper is divided into five sections. In the next section, we give the averaged conservative equations of the orbital and precessional motions and reformulate the influence of obliquity–oblateness feedback on the mean obliquity of the Earth. In section three, we calculate the time-dependant variations of the dynamic ellipticity used for the Plio-Pleistocene glaciations and numerical integrations. This includes the choice of a non-linear ice volume model to insolation forcing and of a viscous internal flow model. Section four summarizes numerical integrations and comparisons with the theoretical secular obliquity change. We also discuss the sensitivity of the secular change to input parameters as well as the influence of the obliquity modulation. In section five, we apply this theory to the Permo-Carboniferous and Neoproterozoic glaciations. The previous climate friction scenario of Williams *et al.* (1998) and the high obliquity scenario of Williams (1975) are discussed as well

as the impact of low-latitude glaciations on the secular obliquity change.

2 EQUATIONS OF PRECESSION

2.1 Orbital and rotational dynamics

We suppose that the Earth is a homogeneous rigid body with principal moments of inertia $A \leq B < C$, and that the axis of rotation coincides with the principal axis of inertia. The variations of the precession quantities (see Fig. 1) driven by the planetary perturbations and by luni-solar torques on the equatorial bulge, are determined by the two motions of the equatorial and ecliptic pole. In a rigid-Earth theory (Kinoshita 1977; Laskar 1986; Néron de Surgy & Laskar 1997), the precession equations for the obliquity ε and the precession in longitude ψ are

$$\begin{aligned} \dot{\varepsilon} &= \mathcal{A}(t)\cos\psi - \mathcal{B}(t)\sin\psi \\ \dot{\psi} &= \alpha\cos\varepsilon - \cot\varepsilon\,[\mathcal{B}(t)\cos\psi + \mathcal{A}(t)\sin\psi] - 2\mathcal{C}(t) \end{aligned} \tag{1}$$

with

$$\begin{aligned} \mathcal{A}(t) &= \frac{2}{\sqrt{1-p^2-q^2}}(\dot{q} + p(q\dot{p} - p\dot{q})) \\ \mathcal{B}(t) &= \frac{2}{\sqrt{1-p^2-q^2}}(\dot{p} - q(q\dot{p} - p\dot{q})) \\ \mathcal{C}(t) &= q\dot{p} - p\dot{q} \end{aligned} \tag{2}$$

and where

$$\begin{aligned} q &= \sin(i/2)\cos\Omega \\ p &= \sin(i/2)\sin\Omega \end{aligned} \tag{3}$$

are related to the variations of the Earth's inclination and node caused by the gravitational planetary perturbations.

$$\alpha = \frac{3G}{2\omega}\left[\frac{m_\odot}{a_\odot^3\left(1-e_\odot^2\right)^{3/2}} + \frac{m_M}{a_M^3\left(1-e_M^2\right)^{3/2}}\left(1-\frac{3}{2}\sin^2 i_M\right)\right] E_d \tag{4}$$

is called the 'precession constant' and is proportional to the dynamical ellipticity

$$E_d = \frac{C-(B+A)/2}{C} \tag{5}$$

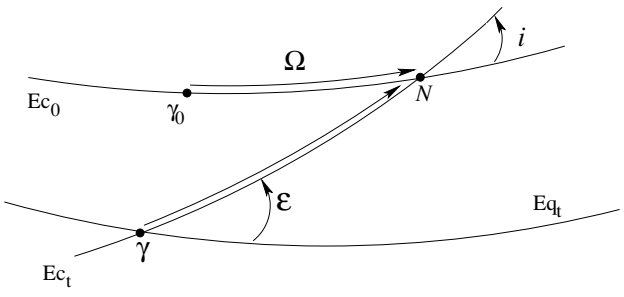

Figure 1. Reference planes for the definition of precession. Eq_t and Ec_t are the mean equator and ecliptic of the date with the spring equinox γ. Ec_0 is the fixed J2000 ecliptic, with equinox γ_0, i is the inclination of the ecliptic Ec_t on Ec_0. The general precession in longitude, ψ is defined by $\psi = \gamma N + N\gamma_0 = \gamma N - \Omega$, where N is the ascending node of the ecliptic of date on the J2000 reference fixed ecliptic. ε denotes the obliquity.

which expresses the departure from spherical symmetry of the mass distribution. $E_d(t)$ is variable, since moments of inertia may be changed by mass redistribution both on and within the Earth, during glaciation–deglaciation processes. G, $m_\odot$, $a_\odot$, $e_\odot$, m_M, a_M, e_M, i_M are respectively the gravitational constant, the masses, the semi-major axes, the eccentricities and the inclinations of the Sun and the Moon while ω is the rotational angular velocity of the Earth. We introduce the gravitational harmonic coefficient of degree 2

$$J_2 = \frac{C-(B+A)/2}{M_e R^2} \tag{6}$$

which is related to the dynamical ellipticity by the dimensionless factor C/M_eR^2 where M_e and R are respectively the mass and the mean equatorial radius of the Earth. Our initial dynamic ellipticity value $E_d^0 = 0.003280165$ is adjusted in eq. (1) to fit at the origin J2000 the observed initial conditions for the speed of precession and obliquity:

$$\dot{\psi}|_{t=0} = 50.290966'' \text{ yr}^{-1} \tag{7}$$

$$\varepsilon_0 = 23^\circ 26' 21''.448, \tag{8}$$

following (Laskar 1986; Laskar *et al.* 1993).

For our integrations of the precession equations, the complex planetary perturbation function $\mathcal{A} + i\mathcal{B}$ issued from the secular orbital solution La90 (Laskar 1988, 1990) was approximated by its quasi-periodic form over 5 Myr

$$\mathcal{A}(t) + i\mathcal{B}(t) \simeq \sum_{k=1}^{N} a_k e^{i(\sigma_k t + \theta_k)} \tag{9}$$

truncated to the twenty largest terms with the frequency analysis method of Laskar (1993). The frequencies σ_k are known to be linear combinations of the fundamental secular frequencies s_j and g_j of the Solar System secular solution (Laskar 1990). Although a quasi-periodic approximation does not provide an accurate representation of the Earth's orbital motion (Laskar *et al.* 1993) as this motion is chaotic (Laskar 1990), it provides here a sufficient framework to study the obliquity evolution. In order to further estimate the obliquity evolution in the presence of ice-age perturbations, we linearize the precession equations at different orders. At zero order, which corresponds to an absence of planetary perturbations, the precession eqs (1) are reduced to

$$\begin{aligned} \dot{\varepsilon} &= 0 \\ \dot{\psi} &= \alpha\cos\varepsilon = p, \end{aligned} \tag{10}$$

implying constant obliquity and spin precession rate values. In that case, the precession angle ψ follows a linear evolution $\psi(t) = p \times t + \psi_0$ with time. At first order, the obliquity variations can be written from (1) and (9) as

$$\dot{\varepsilon} = \sum_{k=0}^{N} a_k \cos(\sigma_k t + \theta_k + \psi). \tag{11}$$

Keeping the zero order approximation for the precession rate (10), eq. (11) is integrated in

$$\varepsilon(t) = \bar{\varepsilon} + \sum_{k=1}^{N} \frac{a_k}{p+\sigma_k}\cos[(p+\sigma_k)t + \theta_k - \pi/2]. \tag{12}$$

Concurrently, we constructed a nominal obliquity solution, based on a numerical integration of eq. (1) over 5 Myr with a constant

Table 1. The seven major terms of the quasi-periodic approximation of the obliquity, $\varepsilon(t) = \sum_{k=0}^{N} \varepsilon_k \cos(\nu_k t + \Psi_k)$ over 5 Myr. The frequency p denotes the mean spin precession rate.

Origin	ν_k ($''$ yr^{-1})	Period (yr)	ε_k (rad)	Ψ_k ($^\circ$)
–	0.0000	–	0.406123	0.000
$p + s_3$	31.6189	40988	0.009856	63.866
$p + s_4$	32.7126	39617	0.004363	99.631
$p + s_3 + g_4 - g_3$	32.1767	40276	0.003482	69.933
$p + s_6$	24.1399	53687	0.002918	−52.241
$p + s_3 - g_4 + g_3$	31.0898	41657	0.002557	−145.265
$p + s_2$	43.5215	29778	0.001422	−124.677
$p + s_1$	44.8688	28884	0.001343	−139.846

dynamical ellipticity $E_d = E_d^0$. A quasi-periodic approximation of this solution

$$\varepsilon(t) = \sum_{k=1}^{N} \varepsilon_k \cos(\nu_k t + \Psi_k) \tag{13}$$

is given in Table 1, with the largest seven terms. The astronomical origin of the frequencies ν_k are shown as functions of the mean spin precession rate p and the fundamental secular frequencies s_j and g_j. Major periodicities are close to ∼41 kyr with an additional ∼53.7 kyr cycle. Comparison of (12) and (13) shows that:

$$\begin{aligned} \varepsilon_k &= a_k/\nu_k, \\ \nu_k &= p + \sigma_k \\ \Psi_k &= \theta_k - \pi/2. \end{aligned} \tag{14}$$

Although these relationships are obtained at very low order of approximation, we will assume that they are still valid in the presence of additional ice-age perturbations.

2.2 Obliquity–oblateness feedback

Let us consider now the effect of ice-age perturbations on the obliquity motion. During glacial cycles, mass transport between the oceans and continental ice sheets and the viscous deformation of the Earth in response to the surface loading and unloading processes, produce perturbations in the dynamic ellipticity of the Earth. The departure of the precession constant α from its mean value $\overline{\alpha}$ may be written as

$$\alpha(t) = \overline{\alpha} + \delta\alpha(t). \tag{15}$$

As the amplitude of the obliquity oscillations (∼1.3°) around its mean value $\overline{\varepsilon}$ is small, the spin precession rate from (10) and (15) yields to first order:

$$\dot{\psi} = p + \delta\alpha(t) \cos\overline{\varepsilon} \tag{16}$$

where the quasi-periodic fluctuations of the precession constant are written here

$$\delta\alpha(t) \cos\overline{\varepsilon} = \sum_{j=1}^{N'} b_j \cos(\nu_j t + \delta_j), \tag{17}$$

which contain the main frequencies $(\nu_j)_{j=1,N}$ of the obliquity forcing. The complementary frequencies $(\nu_j)_{j=N+1,N'}$ correspond either to other additional orbital contributions (eccentricity, climatic precession) or to internal frequencies of the glacial variability. In that case, an integration of (16), (17) and its insertion in (11) yields

$$\dot{\varepsilon} = \sum_{k=1}^{N} a_k \cos\left[\nu_k t + \theta_k + \sum_{j=1}^{N'} \frac{b_j}{\nu_j} \sin(\nu_j t + \delta_j)\right], \tag{18}$$

using $p + \sigma_k = \nu_k$, that is $\dot{\varepsilon} = Re(h(t))$, with

$$h(t) = \sum_{k=1}^{N} a_k e^{i(\nu_k t + \theta_k)} \prod_{j=1}^{N'} e^{i\frac{b_j}{\nu_j}\sin(\nu_j t + \delta_j)}. \tag{19}$$

If we introduce the Bessel functions J_n of order n defined for two reals a and b by

$$e^{ia\sin b} = \sum_{n=-\infty}^{n=+\infty} J_n(a) e^{inb}, \tag{20}$$

we obtain

$$h(t) = \sum_{k=1}^{N} a_k \left[e^{i(\nu_k t + \theta_k)} \prod_{j=1}^{N'} \left(\sum_{n=-\infty}^{n=+\infty} J_n\left(\frac{b_j}{\nu_j}\right) e^{i(n\nu_j t + n\delta_j)} \right) \right]. \tag{21}$$

We then average formally eq. (21). More precisely, for all $j = 1, N'$, $\nu_j t$ is replaced by an independent angle ϕ_j in (21), and the average is made over all angles ϕ_j. Practically, in the absence of additional resonances[1], this is close to the result obtained by averaging (21) with respect to t, over a time interval much larger than the main obliquity periods. All periodic terms in the formal angles ϕ_j will disappear and the only part that remains are the terms independent of the ϕ_j, obtained when $k = j$ and $n = -1$ in (21), i.e.

$$\langle\dot{\varepsilon}\rangle = \langle Re(h(t))\rangle = \sum_{k=1}^{N} a_k J_{-1}\left(\frac{b_k}{\nu_k}\right) \cos(\theta_k - \delta_k). \tag{22}$$

As $b_k/\nu_k \ll 1$, we develop the Bessel function J_{-1} at first order: $J_{-1}(x) = -x/2 + \mathcal{O}(x^3)$. Finally, using (14), eq. (22) gives an estimation of the secular change of the mean obliquity:

$$\frac{d\overline{\varepsilon}}{dt} = \frac{1}{2} \sum_{k=1}^{N} b_k \varepsilon_k \sin(\Psi_k - \delta_k). \tag{23}$$

This simplified expression, where (ε_k, ψ_k) and (b_k, δ_k) are defined in (13) and (17), is similar to the initial analysis of Rubincam (1993) and will be used in the present work. The more general formulation (21) should be used in extreme cases, when the approximation $b_k/\nu_k \ll 1$ is not valid. If the obliquity and the oblateness oscillations are exactly in phase ($\delta_k = \Psi_k$), there is no long-term effect. The secular obliquity change thus only depends on the amplitudes (b_k) and on the phases $(\Psi_k - \delta_k)$ of the oblateness variations in the obliquity band.

3 DYNAMICAL ELLIPTICITY DURING AN ICE-AGE

To estimate the secular obliquity change, the components of the variations of the Earth's oblateness due to obliquity forcing are required. The perturbations of the dynamical ellipticity E_d associated

[1] We will say that an additional resonance occurs if the non-linear glacial response to the insolation forcing produces sub-harmonics terms of frequency $\nu_{k_p} = \nu_k/p$. For each of these terms, we would have an additional resonant term for $n = -p$, of the form $a_{k_p} J_{-p}(\frac{b_{k_p}}{\nu_{k_p}}) \cos(\theta_{k_p} - p\delta_{k_p})$. Although this phenomena may exist, it is assumed to be small and will be neglected in the following.

with small variations in the three principal moments of inertia of the inertia tensor are given by (5) as

$$\delta E_d = (1 - E_d)\frac{\delta C}{C} - \frac{\delta A + \delta B}{2C}. \tag{24}$$

Since the trace of the inertia tensor is invariant under a broad class of Earth's material deformations (Rochester & Smylie 1974), we have $\delta A + \delta B + \delta C = 0$. Substitution into (24) and retaining only first order terms then leads to

$$\frac{\delta E_d}{E_d^0} \sim \frac{3}{2}\frac{\delta C}{C_0 E_d^0}, \tag{25}$$

where C_0 is the present-day observed value of C. For a viscoelastic Earth, the total perturbation of the polar inertia consists of the contribution $\delta C^R(t)$ due to the direct effect of the change in the surface load, assuming that the Earth is perfectly rigid, and of the contribution $\delta C^S(t)$ due to the indirect effect of the Earth's interior compensating flow. Adding these contributions, the polar inertia perturbation is written here as

$$\delta C(t) = \delta C^R(t) + \delta C^S(t). \tag{26}$$

3.1 Ice-sheet orbital coupling

In general, an accurate computation of glaciation-induced inertia perturbations requires detailed data on the space and time evolution of the ice and ocean loading histories. This is unfortunately not available prior to the Last Glacial Maximum (LGM) (about 20 kyr ago), and even less known for Pre-Pleistocene ice ages. A number of models have been proposed for the ice loading history since the LGM (e.g. Denton & Hughes 1981; Tushingham & Peltier 1991; Peltier 1994), mainly associated with the complete disintegration of the Laurentian and Fennoscandian ice complexes along with much of the West Antarctic ice sheet. The end of the deglaciation event is presumed to have occurred approximately 6 kyr ago. With the evident lack of constraints on the spatio-temporal ice loading history during the Plio-Pleistocene glaciations, and as our goal is to give some constraints and properties of climate friction effect, we used a simplified approach. For Plio-Pleistocene glaciations and forward numerical integrations, we assume that the boundaries of the ice sheets remained the same as those at the LGM, and that the instantaneous ice thickness is proportional to the ice volume. By making this approximation, we ignore the potential changes in the surface area of the ice sheets as their volume varies through time. However, as the polar inertia is only related to the projection of the ice load onto the spherical harmonics of degree 2, the influence of the uncertainties in the polar ice partitioning is significantly less important than the total ice-mass or volume fluctuations. If we assume that during the glaciation–deglaciation process the ice sheets discharge their meltwater or accrete water uniformly from the complementary oceans, the polar inertia perturbation, arising from both ice sheet and ocean contributions is, at first order, proportional to the ice volume perturbation (Wu & Peltier 1984):

$$\delta C^R(t) = \gamma\left(V_{\rm ice}(t) - V_{\rm ice}^0\right). \tag{27}$$

where $V_{\rm ice}^0$ is the present global ice volume, and γ is a proportionality coefficient. For each ice volume history, we calibrated the γ parameter by using the polar inertia change ΔC^R and the ice volume change $\Delta V_{\rm ice}(<0)$ over the last deglaciation event since the LGM. In that case, we have

$$\delta C^R(t) = \frac{\Delta C^R}{\Delta V_{\rm ice}}\left(V_{\rm ice}(t) - V_{\rm ice}^0\right). \tag{28}$$

We estimated the ΔC^R value on the basis of the recent deglaciation models ICE-3G (Tushingham & Peltier 1991) and ICE-4G (Peltier 1994) which satisfy geophysical data and constraints associated with relative sea level variations since the LGM. Theses models include a complementary ocean loading history based on a self-consistent sea level equation. From the ICE-4G model, Jiang & Peltier (1996) estimated a polar inertia change very close to 1.0×10^{33} kg m^2, which is slightly larger than the 0.846×10^{33} kg $\cdot$ m^2 inferred with the ICE-3G model (Mitrovica & Forte 1995). Each ice load model corresponds to a relative change of the Earth's oblateness

$$\frac{\Delta J_2^R}{J_2^0} = \frac{3}{2}\frac{\Delta C^R}{J_2^0 M_e R^2}, \tag{29}$$

of respectively $\sim$0.570 per cent and 0.482 per cent (which correspond to rigid-Earth values). This corresponds to approximately $\sim 50.10^6$ km^3 of ice which has melted from the land-based ice sheets, raising global sea level by $\sim$130 m. Previous estimates of this quantity, based on a decoupling between ice and ocean loading histories and spherical caps approximation, are close to 0.46 per cent (Wu & Peltier 1984; Peltier 1989). These are somewhat larger than the 0.33 per cent and 0.3 per cent values respectively used by Rubincam (1995) and Ito *et al.* (1995) with simplified glacial palaeotopography. During a deglaciation stage, water-ice masses are transferred from the polar regions to the global oceans, increasing the polar moment of inertia ΔC^R and hence ΔJ_2^R. The situation is reversed for predominantly low-latitude glaciations producing a negative change of oblateness. Putting all the ice mass at the pole or at the equator maximizes the oblateness change. Waxing and waning of sea ice, floating in the ocean, has no influence on sea level or oblateness changes.

It is widely accepted that past variations of global continental ice volume or eustatic sea level are generally well approximated by δ^{18}O oxygen-isotope records from benthic marine sediments (Shackleton 1967). This assumption has received large support from independent sea level histories obtained from fossil coral terraces (Chappell & Shackleton 1986). However, the complete obliquity–oblateness feedback requires ice-sheet models which are coupled to orbital and insolation/obliquity changes. Our calibration (28) also requires an ice volume model that matches, at least approximately, the last glacial cycles.

In previous studies, Ito *et al.* (1995) and Williams *et al.* (1998) used a linear relationship between the ice volume and the summer insolation forcing at northern high latitudes, based on the historical Milankovitch assumption. Although the summer insolation appears to be strongly correlated with some Pleistocene climatic proxy records (Hays *et al.* 1976; Imbrie *et al.* 1992, 1993), the predominance of a $\sim$100 kyr cyclicity during the Late Pleistocene and of the 41 kyr cycle during the Late Pliocene-Early Pleistocene provide evidence that the ice volume response cannot be related to the climatic precession-dominated 65°N summer insolation forcing by a simple linear mechanism.

Most of the models of ice-sheet response to orbital forcing have focused on the onset and the predominance of the $\sim$100 kyr cycle at the mid-Pleistocene transition (see Imbrie *et al.* 1993; Paillard 1998). The amplification in the presumed eccentricity band is generally simulated by internal non-linear interactions between the orbitally-forced response and the dynamics of oceans, ice sheets and the lithosphere. These interactions include positive feedbacks involving the ice albedo effect, the interplay between ice accumulation and surface elevation (Gallée *et al.* 1992), and the long time response associated with massive ice sheets (Imbrie *et al.*

1993). It is thus very likely that similar non-linear effects could have occurred during more severe past glacial episodes.

Our study is based on the non-linear model of Imbrie & Imbrie (1980), in which the non-linearity is produced by an asymmetry between an unstable fast deglaciation process (termination) and a slow ice accumulation. This is consistent with the asymmetric pattern of the 100 kyr cycles which, at first order, exhibits a ∼90 kyr slow accretion time followed by a rapid ∼10 kyr disintegration. In insolation units, the variable V, which is linearly related to the ice volume, follows a simple first-order relaxation to the insolation forcing of reference $I_{\rm ref}$ with a different time constant depending on the sign of ice volume changes. The equation is

$$\frac{dV}{dt} = \frac{(I_{\rm ref} - V)}{\tau}, \tag{30}$$

where $\tau = \tau_M$ if $I_{\rm ref} > V$ (melting) and $\tau = \tau_A$ otherwise (accumulation). The time constants τ_A and τ_M can be respectively written as

$$\tau_A = \frac{T_m}{1-b}; \tau_M = \frac{T_m}{1+b} \tag{31}$$

where T_m is the mean time constant of the ice system and b, a non-linearity coefficient ($0 < b < 1$). In the original paper (Imbrie & Imbrie 1980), the insolation forcing $I_{\rm ref}$ is classically the summer insolation at 65°N, $\tau_A = 42.5$ kyr and $\tau_M = 10.6$ kyr which corresponds to $T_m = 17$ kyr, $b = 0.6$ and a ratio $\tau_A/\tau_M = 4$. This provides our nominal ice volume model. In that case, the last glacial cycles are fairly well reproduced, although a strong 400 kyr cyclicity is present, without a clear 100 kyr cyclicity. A quasi-periodic approximation of the nominal ice volume model over the next 5 Myr is given in Table 2. Over that time interval, the ice volume model variability is mainly dominated by the 41 kyr obliquity cycle, the ∼23 kyr (∼23.7 and 22.3 kyr) climatic precession cycles and the ∼400 kyr eccentricity cycle. In the obliquity band, the ∼54 kyr obliquity cycle has a larger amplitude than the other minor ∼41 kyr cycles, in comparison with the direct obliquity forcing (see Table 1), that illustrates its low-pass filtering effect. For an input frequency ν of the insolation forcing, the average phase lag of the ice volume output component is closer to the phase lag $\tan^{-1}(\nu \times \tau_A)$ of the accumulation stage than the lag $\tan^{-1}(\nu \times \tau_M)$ of the melting stage, since the model predicts a longer glacial than interglacial interval. In any case, the phase lag is lower than 90°.

Although the last glacial cycles are roughly well reproduced, to which extent a such model can describe the glacial response to insolation forcing for Pre-Pleistocene glaciations, which are poorly known, is uncertain. For this reason, we have considered the Imbrie and Imbrie model only as a conceptual model of ice volume response to insolation forcing, in which all the non-linear effects are lumped into the analytical forms (30) and (31). It is thus possible to test the properties and the impact of climate friction by modifying the ice volume response parameters for different glacial configurations. In particular, changes in τ_M and τ_A values can modify the phase lag between the obliquity components of the ice volume fluctuations and the obliquity forcing. The degree of non-linearity can be simply controlled by the b parameter value. The forcing insolation $I_{\rm ref}$ can be also adapted to the latitudinal extent of the glaciations.

3.2 Viscoelastic relaxation of the Earth

The second input required to compute the response of the Earth to glaciation–deglaciation events is a viscoelastic model of the planet's interior. An appropriate model is determined by the viscosity profile coupled with the seismically determined profiles of density and elastic parameters. The relaxation process associated to the surface loading of a spherical harmonic component of degree 2 is based upon a linear viscoelastic field theory which describes the induced deformation of a self-gravitating and spherically symmetric viscoelastic Earth (Peltier 1974, 1985). In the time domain, the inertia deformation response depends not only on the present surface loading $\delta C^R(t)$ but also on its past history through the time convolution:

$$\delta C^S(t) = k_2^L * \delta C^R(t), \tag{32}$$

where $k_2^L(t)$ are the surface load Love number of degree 2. For a multi-layered radially stratified Earth with Maxwell rheology, the relaxation process is characterized by an immediate elastic effect with the 'amplitude' $k_2^{L,E}$ (here ~ -0.3) and a set of M normal modes of pure exponential decay with the decay times s_j and the amplitudes r_j (Peltier 1985):

$$k_2^L(t) = k_2^{L,E}\delta(t) + \sum_{j=1}^{M} r_j e^{-s_j t}, \tag{33}$$

where $\delta(t)$ is the Dirac function. The poles $s_j(>0)$ and the residues r_j are found by solution of the appropriate boundary value problems (Peltier 1985). Each discontinuity in density induces an additional buoyancy mode, while each discontinuity in rigidity or viscosity will induce two additional modes.

Table 2. The main terms of the quasi-periodic approximation of the ice-volume model of Imbrie & Imbrie (1980) in insolation units, $V(t) = \sum_{j=0}^{N''} V_j \cos(\nu_j t + \delta_j)$ over 5 Myr and their astronomical origin. The first column gives the position (j) of each frequency ν_j in the quasi-periodic development. For $j > 7$, only the obliquity frequencies are given. The real ice-volume function is a linear function of $V(t)$ but its determination is here not necessary.

j	Origin		ν_j ($''$ yr^{-1})	Period (yr)	V_j (W m^{-2})	δ_j (°)
0	Mean value		–	–	477.952	−0.0001
1	Obliquity	$p + s_3$	31.541	40986	2.497	−10.395
2	Climatic precession	$p + g_5$	54.702	23685	2.290	4.650
3	Eccentricity	$g_2 - g_5$	3.191	405402	2.147	147.282
4	Climatic precession	$p + g_2$	57.929	22372	1.821	169.237
5	Climatic precession	$p + g_4$	68.394	18948	1.338	110.145
6	Eccentricity	$g_4 - g_2$	10.454	123965	1.051	−109.425
7	Eccentricity	$g_4 - g_5$	13.681	94729	1.046	38.909
8	Obliquity	$p + s_6$	24.156	53651	1.045	−142.144
10	Obliquity	$p + s_4$	32.723	39604	1.020	17.076
13	Obliquity	$p + s_3 + g_4 - g_3$	32.174	40280	0.812	−4.863
16	Obliquity	$p + s_3 - g_4 + g_3$	31.087	41689	0.605	−126.574

We used the four-layered models described in Wu & Peltier (1984) which include the 1066B elastic structure of Gilbert & Dziewonski (1975). We have considered two different viscosity profiles, each with a constant upper-mantle viscosity $\nu_{\rm UM} = 10^{21}$ Pa s, and an elastic lithosphere of 120.7 km thickness. The model B has a $\nu_{\rm LM} = 3.10^{21}$ Pa s lower mantle viscosity value, as required by observations related to postglacial rebound (e.g. Mitrovica & Peltier 1993), and which is slightly larger than for the model A ($\nu_{\rm LM} = 10^{21}$ Pa s). For a forward integration, the time convolution operation from (32) and (33) is

$$\delta C^S(t) = k_2^{L,E}\delta C^R(t) + \sum_{j=1}^{M} r_j \int_{-\infty}^{t} \delta C^R(t') e^{-s_j(t-t')}\, dt'. \qquad (34)$$

The elastic response of the planet acts immediately to compensate approximately about 30 per cent of the inertia perturbations induced by surface mass redistribution. The additional viscous adjustment tends to compensate the remaining fraction $(1 + k_2^{L,E})$ with time. To describe the viscous relaxation process as a delayed response to the surface loading, we followed the approach of Ito *et al.* (1995). For a single sinusoidal periodic forcing with an unity amplitude $\delta C^R(t) = \sin(\nu t)$, the amplitude and the phase of the viscous response, i.e. the second term of (34), is given by

$$\sum_{j=1}^{M} r_j \int_{-\infty}^{t} \sin(\nu t') e^{-s_j(t-t')}\, dt' = -\mathcal{A}_s(\nu)\sin[\nu t - \zeta_s(\nu)] \qquad (35)$$

where the amplitude of the response is

$$\mathcal{A}_s(\nu) = \sqrt{\left(\sum_{j=1}^{M} \frac{-r_j s_j}{(s_j)^2 + \nu^2}\right)^2 + \left(\sum_{j=1}^{M} \frac{-r_j \nu}{(s_j)^2 + \nu^2}\right)^2} \qquad (36)$$

and the viscous phase lag $\zeta_s(\nu)$ is

$$\zeta_s(\nu) = \tan^{-1}\left[\frac{\sum_{j=1}^{M} \frac{-r_j \nu}{(s_j)^2+\nu^2}}{\sum_{j=1}^{M} \frac{-r_j s_j}{(s_j)^2+\nu^2}}\right]. \qquad (37)$$

The long-term load response of the viscous part is then

$$\lim_{\nu\to 0} \mathcal{A}_s(\nu) = -\sum_{j=1}^{M} \frac{r_j}{s_j} \simeq 1 + k_2^{L,E} \qquad (38)$$

owing to the fact that $1 + k_2^{L,E} + \sum_{j=1}^{M} r_j/s_j \sim 0$ (Wu & Peltier 1984). The very slight departure from zero (0.009 for the model B) is known to arise from the presence of the elastic lithosphere which prevents the complete isostatic compensation at long periods (Wu & Peltier 1984). The normalized gain $f(2\pi/\nu) = \mathcal{A}_s(\nu)/\mathcal{A}_s(\nu = 0)$ and the phase functions for both models A and B are illustrated in Fig. 2 as a function of the loading period $(2\pi/\nu)$. For very large loading periods ($2\pi/\nu > 10^6$ yr), the viscous Earth completely follows the perturbation without phase lag, and the inertia compensation is nearly complete. In contrast, short loading periods ($2\pi/\nu < 10^3$ yr) lead to very weak inertia compensation with a nearly 90° phase lag. The relaxation process acts like a low-pass filter in which low-frequency oscillations are transmitted unattenuated and in phase. For characteristic obliquity and other Milankovitch periods ($\sim 10^4$–10^5 yr), phase lags are in a 15–40° range with a 22.5° lag for a 41 kyr loading cycle with the model B, which falls to 12.2° with the model A. The corresponding gains are in a 0.4–0.85 range that corresponds to the most sensitive part of the Earth's interior response. Comparison between models A and B shows that the phase lag and the gain are respectively increasing and decreasing functions of the lower mantle viscosity, indicating, as expected, that the

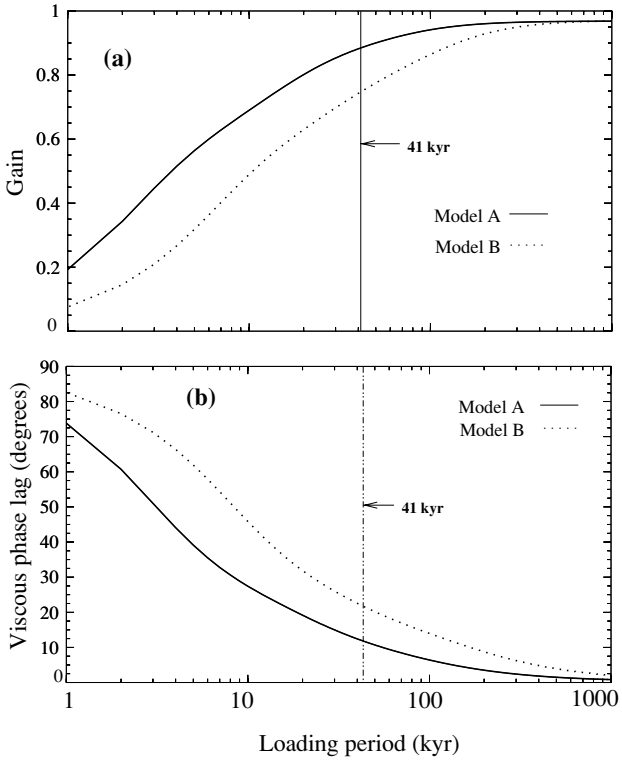

Figure 2. (a) Viscous gain $f(2\pi/\nu) = \mathcal{A}_s(\nu)/\mathcal{A}_s(\nu = 0)$ as a function of the loading period for both viscoelastic models A (solid line) and B (dashed line). (b) As in (a) but for the viscous phase lag ζ_s in degrees.The vertical line indicates the present main obliquity 41 kyr cycle.

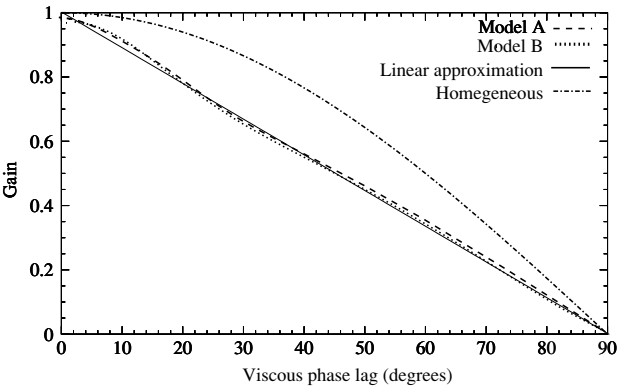

Figure 3. Gain f as a function of the viscous phase lag ζ_s for different viscoelastic models. The models A (dashed line) and B (dotted line) are plotted with the linear function $f(\zeta_s) = 1 - \zeta_s/90°$ (solid line). The homogeneous mantle case corresponds to $f(\zeta_s) = \cos(\zeta_s)$ (dashed-dotted line).

isostatic compensation process becomes less rapid for a higher viscosity mantle. For both models, the gain f is plotted as a function of the phase lag ζ_s in Fig. 3 and in comparison with the Darwin model case corresponding to a simple homogeneous and incompressible mantle. This latter case was studied by Rubincam (1995), leading to the analytical gain: $f(\zeta_s) = \cos(\zeta_s)$. Stratified models A and B exhibit significant differences with the simple Darwin model. In particular, for a given phase lag, stratified models respond with a lower gain than Darwin model, that is consistent with the mechanical analysis of Spada & Alphonsi (1998). Furthermore, Fig. 3 indicates

that for both viscoelastic models A and B, the gain f can be well approximated by the simple linear function

$$f(\zeta_s) \simeq 1 - \zeta_s/90^\circ, \tag{39}$$

where ζ_s is expressed in degrees. This relationship appears to be thus independent of the lower mantle viscosity $\nu_{\rm LM}$, and we will assume that eq. (39) holds also for other values of $\nu_{\rm LM}$. This contrasts significantly with the previous study of Ito *et al.* (1995) and thereby Williams *et al.* (1998) which described the inertia relaxation with the radial surface Love numbers h_2^L and found a non-monotonic behaviour of the gain with the viscous phase lag.

3.3 Secular change of obliquity

We can combine the previous contributions to the net change of dynamic ellipticity during an ice-age and extract the periodic components related to the obliquity forcing. Substitution of the surface mass loading (28) into (34) and adding both contributions gives the global perturbation in the polar inertia

$$\delta C(t) = \frac{\Delta C^R}{\Delta V_{\rm ice}} \left[\left(1 + k_2^{L,E}\right) V_{\rm ice}(t) + \sum_{j=1}^{M} r_j \int_{-\infty}^{t} V_{\rm ice}(t') e^{-s_j(t-t')}\, dt' \right]. \tag{40}$$

Assuming that the ice volume can be approximated by a quasi-periodic function

$$V_{\rm ice}(t) = \sum_{j=1}^{N'} V_j \cos(\nu_j t + \delta_j) \tag{41}$$

and using (25), (29), (35) and (40), we obtain:

$$\delta\alpha(t)/\alpha_0 = -\frac{\Delta J_2^R}{2J_2^0} \sum_{j=1}^{N'} \Theta_j \left[\left(1 + k_2^{L,E}\right) \cos(\nu_j t + \delta_j) - \mathcal{A}_s(\nu_j) \cos(\nu_j t + \delta_j - \zeta_s(\nu_j)) \right] \tag{42}$$

similar to the required form (17) and where

$$\Theta_j = \frac{2 \times V_j}{-\Delta V_{\rm ice}} \tag{43}$$

are positive and dimensionless parameters expressing the contribution in amplitude of the frequency ν_j in the ice volume variations, normalized to the global ice volume change over the last deglaciation event. This latter cycle is nearly the largest cycle in amplitude of the Plio-Pleistocene glaciations, and it is expected that Θ_j are always lower than unity. Finally, using (17) and (23) and considering only the resonant obliquity components, the secular variation of obliquity in a linear approximation is

$$\frac{d\bar{\varepsilon}}{dt} = \frac{\Delta J_2^R}{J_2^0} \frac{\overline{\alpha} \cos\bar{\varepsilon}}{4} \left(1 + k_2^{L,E}\right) \times \sum_{k=1}^{N} \Theta_k \varepsilon_k \left[\sin\left(\zeta_i^k\right) - f(\nu_k) \sin\left(\zeta_i^k + \zeta_s(\nu_k)\right) \right] \tag{44}$$

where ζ_i^k are the phase lags $(\Psi_k - \delta_k)$ between the periodic components of the obliquity oscillations forcing and the corresponding ice volume components. As an example, ζ_i^1 corresponds to the phase lag between the 41 kyr obliquity maxima and the 41 kyr related ice volume minima. All the climate friction mechanism occurs in the obliquity band and it is important to remind that this phase lag is thus not the phase lag between the insolation maxima and the corresponding global ice volume minima as it is used in Williams *et al.* (1998). The sum $\zeta_i^k + \zeta_s(\nu_k)$ corresponds to the phase lags between the obliquity oscillations and the indirect internal mass redistribution.

Our theoretical rate (44) presents significant differences with the previous formulations of Rubincam (1993, 1995) and Ito *et al.* (1995) used by Williams *et al.* (1998). The presence of an elastic lithosphere, which contributes to a large (~30 per cent) and immediate part of the Earth's compensation, similarly affects the secular obliquity change. In Rubincam (1993, 1995), the relative oblateness change $\Delta J_2^R/J_2^0$ is calculated only for half of the total obliquity amplitude, so that the obliquity change is here divided by a factor two. We have also introduced the obliquity-contribution parameters Θ_k. In contrast, Ito *et al.* (1995) and Williams *et al.* (1998) assumed that the global ice volume variations were entirely driven by the obliquity, while the secular drift is proportional only to the fraction of the global ice volume which is driven by the obliquity changes. For numerical integrations, Ito *et al.* (1995) and Williams *et al.* (1998) 'calibrated' the amplitude of the net dynamic-ellipticity perturbation (with the solid-Earth response included) with a rigid-Earth value, while we showed that the two stages must be separated. It results in the amplitude of their time-dependent inertia perturbations being quite similar to that of a rigid planet. This explains the inconsistency (and the overestimation) between the previous theoretical and computed secular obliquity changes.

Finally, it should be stressed that the secular response of the obliquity (22) does not depend on the complete response of the climate model (given by the terms in all the harmonics ν_j, for $j = 1, N'$), but only on its response in the obliquity band (limited to the sole harmonics ν_j, for $j = 1, N$). It is thus only necessary to analyse whether the climate response in the obliquity-band is realistic.

4 CONSTRAINTS AND PROPERTIES OF CLIMATE FRICTION DURING PLIO-PLEISTOCENE GLACIATIONS

In this section, we report the numerical integrations made with the Imbrie and Imbrie ice volume model (Imbrie & Imbrie 1980) in order to compare those with the theoretical expression (44). We then explore in detail the sensitivity and the properties of the secular obliquity change during the recent and documented Plio-Pleistocene glaciations using more direct constraints issued from benthic oxygen-isotope records. This allows us to discuss the limitations of the ice volume model used in our numerical integrations, but also to give some realistic boundaries for the climate friction effect during the recent glaciations. These results will serve as a guide for Pre-Cenozoic glaciations, which are much less constrained.

4.1 Influence of the ice sheet phase lag

Phase lag relationships between astronomical cycles and their induced climatic variations play a central role in the understanding of the climatic response to orbital forcing and in the subsequent astronomical calibration of climate proxy records. Recent improvements in their determination has allowed the construction of an astronomical time-scale in very good agreement with independent radiometric dating. In the obliquity-band, phase relationships are well established during the Pleistocene, when the thermal inertia of the large Northern Hemisphere ice sheets sets the phase of the climate response. An average 9 ± 2 kyr lag value ($80 \pm 20^\circ$)

resulting from cross-correlation between the 41 kyr extracted variation of δ^{18}O records from globally distributed marine sediments or ice cores, and obliquity variations was largely used (Imbrie *et al.* 1984, 1992, 1993). An ∼8 kyr lag (70°) seems now a convergent value (Clemens 1999). However, Hilgen *et al.* (1993) pointed out some uncertainties in these estimations that could provide a lower value close to ∼6 kyr. A similar lag value 7 ± 1 kyr is found in the Vostok ice core record (Shackleton 2000) reflecting the hemispherical symmetry of the obliquity forcing. An 8 kyr obliquity lag is usually explained as a first-order relaxation response of continental ice sheets to the obliquity forcing, with a characteristic time constant close to 17 kyr, consistent with the previous mean time constant of the Imbrie and Imbrie model (Imbrie *et al.* 1992). Despite of the complexity of the ice sheet dynamics which involve interactions between accumulation, ablation and glacial flow, its characteristic time constant is likely to be related to its volume. For ice sheets following the simple Paterson volume–size relationship: $[V] \propto [S]^{1.23}$, a scaling analysis suggests that their characteristic time constant is proportional to $V^{1/5}$ (Bahr *et al.* 1998). In that case, small changes of the time constant and hence of phase lag are expected even for large ice volume changes. For Pliocene glacial records, phase relationships in the obliquity band are poorly constrained and global-scale correlative values are still unavailable (Clemens 1999). Therefore, Shackleton *et al.* (1995a) document that a long time constant exists in the Pliocene climate system, suggesting that a similar phase lag should have existed within the Pliocene glaciations. A lower 6 kyr obliquity lag is currently used prior to ∼3 Ma to illustrate the reduced size of the Pliocene ice sheets with respect to the Late Pleistocene (e.g. Lourens *et al.* 1996). However, this lag could have changed through time with the evolution of the Pliocene average ice-volume. Since such similar lag relationships are also unavailable for Pre-Pliocene glaciations, we explored the sensitivity of the secular change of obliquity for a large range of ice sheet lags to obliquity variations.

The secular obliquity given by (44) has been calculated for an ice-volume model which incorporates the five major obliquity-period contributions Θ_k of the nominal Imbrie & Imbrie (1980) model over 5 Myr (see Table 2) but with a free ice sheet phase lag $\zeta_i = \zeta_i^1$ of the main 41 kyr cycle. The isostatic adjustment is based on the viscoelastic model B. With the calibration used,we found a main 41 kyr cycle mean contribution of $\Theta_1 = 41.3$ per cent over 5 Myr. For the other obliquity cycles, we assumed as is well verified in Tables 1 and 2, that the ice time lag $T_i = \zeta_i^1/\nu_1$ is equal for all the obliquity periods of the obliquity band. In that case, we have $\zeta_i^k = \nu_k T_i = \zeta_i^1 \times \nu_k/\nu_1 = \zeta_i \times \nu_k/\nu_1$. It induces only very small variations of the phase lags of the other minor obliquity cycles with respect to the theoretical Imbrie and Imbrie values, since most of the obliquity periods are very close. Only the ∼53.7 kyr is very slightly affected.

The secular obliquity change is plotted in Fig. 4 for characteristically large values of $\Delta J_2^R/J_2^0$. We find that for current positive values of $\Delta J_2^R/J_2^0$, most of the acceptable ζ_i values produce a positive change and only for values $\zeta_i < 44°$ (∼5 kyr) and $\zeta_i > 224°$ (∼26 kyr), the change is negative. As a consequence, the non-intuitive value $\zeta_i = 225°$ invoked in Williams *et al.* (1998) to produce a negative secular change, cancels the secular drift here. It is thus likely that the only realistic way to have a negative drift is that $\zeta_i < 44°$ but it will provide a significant rate only if $\zeta_i \ll 44°$.

For the last deglaciation cycle $\Delta J_2^R/J_2^0 \sim 0.5$ per cent and the current value $\zeta_i = 80°$, we obtain a positive secular drift of 0.0183 deg Myr^{-1}. For our nominal Imbrie & Imbrie (1980) model, a mean phase lag of ∼74° (∼8.4 kyr) is included in the obliquity band.

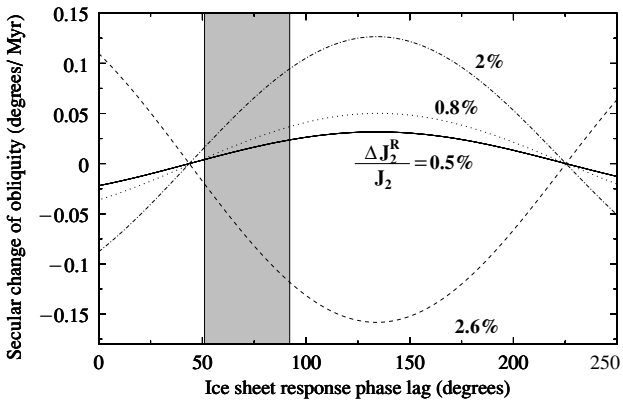

Figure 4. Theoretical secular obliquity drift with the Imbrie & Imbrie (1980) model parameters as a function of the ice sheet response phase lag ζ_i for $\Delta J_2^R/J_2^0 = 0.5$, 0.8 and 2 per cent respective values. A negative value of the rigid change of oblateness (here −2.6 per cent) corresponds to hypothetical low-latitude glaciations which would follow the Imbrie and Imbrie ice volume model evolution. The shaded area corresponds to the range of current values of ζ_i for Plio-Pleistocene glaciations ∼50–90° (∼6–10 kyr). The main-obliquity cycle contribution is 41.3 per cent.

It results in an expected positive secular drift close to 0.0158 deg Myr^{-1}. This rate falls to 0.0142 deg Myr^{-1} for $\zeta_i = 70°$ (∼8 kyr) and to only 0.0097 deg Myr^{-1} for $\zeta_i = 60°$, indicating that in the shaded area of current phase values, the secular obliquity change is very sensitive to the ice sheet phase lag. Note that ∼75 per cent of the previous values comes from the dominant 41 kyr cycle and ∼15 per cent for the second ∼39.6 kyr obliquity cycle. With a very large change of oblateness of 2 per cent, the maximal secular drift obtained is only 0.125 deg Myr^{-1} for $\zeta_i \simeq 133°$ ($T_i \sim 15.2$ kyr).

4.2 Influence of the relative change of oblateness

We first tested the theoretical proportionality between the secular obliquity change and the relative oblateness change. We computed the complete precession eq. (1) over 5 Myr forward using a quasi-periodic approximation of the planetary perturbations, as described in Section 1. The numerical integrations use the Adams multistep method with a 200 yr step and the Laskar *et al.* (1993) routines. The temporal changes of the dynamic ellipticity that can be written from (38) and (40) as

$$\frac{\delta E_d(t)}{E_d^0} = \frac{\Delta J_2^R}{J_2^0}\left[\sum_{j=1}^{M} r_j \int_{-\infty}^{0} e^{-s_j u}\,\frac{V_{\rm ice}(u+t) - V_{\rm ice}(t)}{\Delta V_{\rm ice}}\,du\right] \quad (45)$$

have been included. The ice-volume model of Imbrie & Imbrie (1980) from eq. (30) is simultaneously integrated with the summer insolation at 65°N computed with the La93 solution (Laskar *et al.* 1993). Fig. 5 shows the computed differences in obliquity over 5 Myr relative to the nominal solution ($E_d = E_d^0$) for four different values of oblateness change: 0.2 per cent, 0.5 per cent, 0.8 per cent and 2 per cent. Phase shifts with increasing amplitudes due to glaciation-induced perturbations in the precession angle and hence in the obliquity periodicities are observed between the obliquity solutions. An additional positive secular trend is clearly visible and for each curve the linear trend is plotted. We reproduced the secular obliquity change obtained over 5 Myr for the four previous values and both viscoelastic models A and B in Fig. 6. The linearity is very closely verified for each model. Moreover, for $\Delta J_2^R/J_2^0 =$ 0.5 per cent and model B, the secular obliquity change obtained is

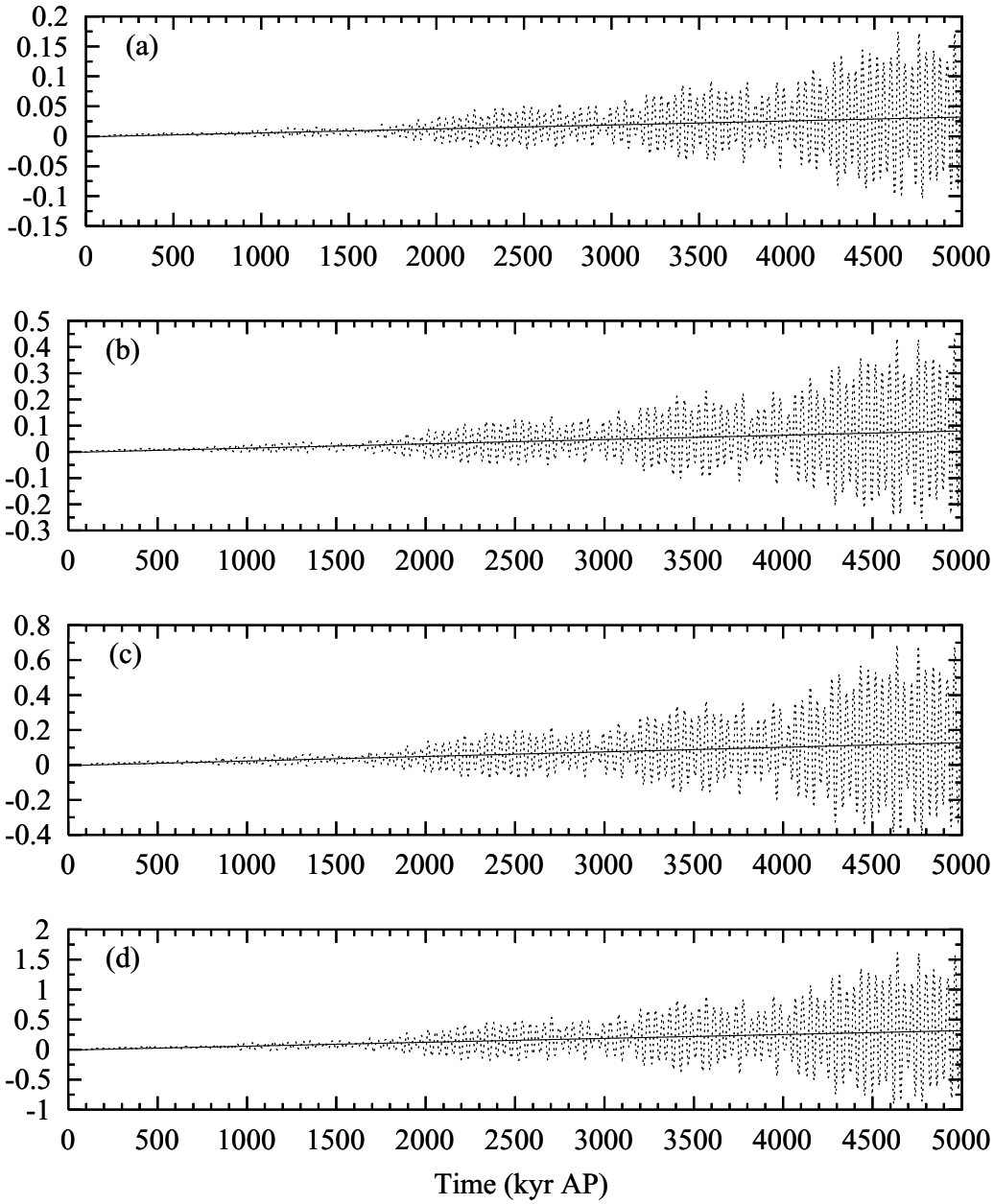

Figure 5. The differences in obliquity fluctuations (in degrees) between the computed obliquity solution incorporating the glaciations-induced perturbations with the Imbrie & Imbrie (1980) ice volume model and the nominal solution with $E_d = E_d^0$ over 5 Myr. (a) The results for $\Delta J_2^R / J_2^0 = 0.2$ per cent (b) 0.5 per cent (c) 0.8 per cent (d) 2 per cent. Each integration includes the viscoelastic model B. A mean $\sim 74^\circ$ phase lag ($\sim$8.4 kyr) is included between the obliquity and the 41 kyr ice-volume variations. For each curve, the linear trend of the signal (solid line) is plotted.

0.0167 deg Myr^{-1} in very good agreement with the previous approximative value 0.0158 deg Myr^{-1} estimated in Section 4.1.

4.3 Influence of the obliquity-driven ice volume

According to eq. (44), the secular obliquity change is proportional to the ice volume driven by each obliquity period through the obliquity contribution parameters Θ_k. It is thus important to investigate if the ice volume model previously used gives an accurate estimate of the ice volume transported by the obliquity variations.

Two phenomena may affect this estimate. First, astronomical-related models predict a climate variability only at orbital and axial frequencies that do not illustrate the large frequency dispersion observed in the ice volume proxy records. Second, if the last deglaciation cycle is not the nearly largest cycle in the Plio-Pleistocene ice volume history, the used calibration may lead to an overestimate of the obliquity contributions parameters. This is the case for the Imbrie & Imbrie (1980) model.

In order to have a more realistic estimate of the obliquity-cycle contributions to the ice volume variations, we have considered a set of high-resolution and long benthic δ^{18}O records collected by the Ocean Drilling Program. They document the major phase of the Northern Hemisphere ice growth, about 3 Ma, marked by the formation of permanent ice sheets at high northern latitudes with

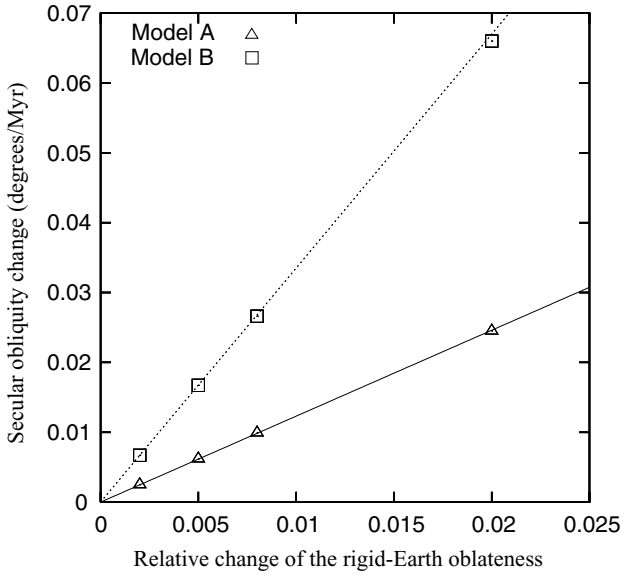

Figure 6. Summary of the computed secular obliquity changes obtained for viscoelastic model A and B as a function of the relative oblateness change $\Delta J_2^R/J_2^0$ (corresponding to a rigid-Earth value) over 5 Myr. The linearity is very well reproduced for each viscoelastic model.

successive glaciations becoming progressively more intense and strongly dominated by the 41 kyr obliquity cycle until the mid-Pleistocene transition (∼800 kyr ago) (e.g. Raymo *et al.* 1989; Tiedemann *et al.* 1994). We also considered the SPECMAP record of Imbrie *et al.* (1984), based on a stacked set of sedimentary core records. We estimated the mean 41 kyr main obliquity cycle contribution Θ_1 for two periods: the Late-Pleistocene (0–780 kyr BP) dominated by the 100 kyr periodicity and for the entire last 3 Myr in Table 3. For each period, the obliquity contribution ranges from ∼22.5 per cent to ∼28.5 per cent indicating nearly constant and correlated climate responses in the obliquity band except for the SPECMAP stack. However, planktonic records are very sensitive to local surface temperature and cannot be used as an accurate global ice volume proxy. Our calculations assume that all the benthic δ^{18}O variability reflects change in global ice-volume. If a significant fraction (∼30 per cent) is generally attributed to deep-sea temperature variations, it does not much affect our estimates as we can reasonably assume that the obliquity contribution associated to ice volume and temperature changes are similar. A mean value of 25 per cent can be reasonably deduced from all the benthic records. This value is similar for the two time intervals, indicating that the mean obliquity-driven ice volume and hence climate friction effect has not much changed during the gradual accumulation of Northern Hemisphere ice sheets since about 3 Ma. This may provide a general constraint on the climate friction amplitude. Even for larger glaciations than at Quaternary, the secular obliquity change may be limited by the incapacity of obliquity variations to remove more ice/water material.

In the same table, we also show the Imbrie & Imbrie (1980) model values and the hypothetical case of a linear correlation between ice volume and summer insolation at 65°N on the same time interval, as used in Ito *et al.* (1995) and Williams *et al.* (1998). It shows the large overestimate of the 41 kyr obliquity-contribution (about twice for the two time intervals) from direct orbital models. If we assume similar proportional decreases of the other obliquity contributions in the ice-volume records with respect to the Imbrie & Imbrie model, the mean secular change of obliquity, estimated to be 0.0183 deg Myr^{-1} for a phase lag $\zeta_i = 80°$ and an obliquity contribution of 41.3 per cent in Section 4.2, becomes approximately only $25 \times 0.0183°/41.3 \simeq 0.011°/\mathrm{Myr}^{-1}$. If we consider only the dominant 41 kyr cycle contribution, this rate is reduced to ∼0.0083 deg Myr^{-1}. These are respectively about 6 and 30 times lower than the rates given in Rubincam (1995) and Ito *et al.* (1995).

4.4 Influence of obliquity modulation

Eq. (44) gives only an averaged value of the secular obliquity change where the obliquity amplitudes ε_k and the obliquity contributions Θ_k are estimated over 5 Myr. We investigate here the properties of the temporal fluctuations of the secular obliquity change over shorter time intervals. For this study, the previous discretization of the obliquity frequencies used in (44) is not appropriate. It is more useful here to come back in the time domain.

Lourens & Hilgen (1997) recently drew attention to the significant correlation between the intervals of high/low amplitude variations of obliquity and the corresponding obliquity-related oxygen isotopic high/low amplitude variations, mainly connected with the ∼1.2 Myr obliquity modulating cycle. This cycle can be associated to the $s_3 - s_4$ frequency (See Table 1 and Laskar 1999). An illustration is

Table 3. Estimation of the mean contribution Θ_1 of the main 41 kyr obliquity cycle in ice-volume proxy benthic oxygen-isotope records since 780 kyr and over the last 3 Myr. Each record was detrended. The mean amplitude of the 41 kyr obliquity component was obtained with the frequency analysis of Laskar (1993) and normalized to the amplitude of the last deglaciation event since the LGM for each record. Similar values for the Imbrie & Imbrie (1980) model are given. Conversely to Imbrie and Imbrie's model, the direct summer insolation at 65°N does not match the last glacial cycles. In the latter case, the obliquity contribution is normalized to the 'equivalent lagged' deglaciation event between ∼ −23 kyr and −9 kyr. It illustrates the large overestimate of the obliquity contribution from orbital forcing models with respect to realistic values inferred from ice volume proxy records.

Site	References	41 kyr contribution Θ_1 (per cent)	
		0–780 ka	0–3 Ma
SPECMAP stack[a]	Imbrie *et al.* (1984)	18.9	–
ODP 849	Mix *et al.* (1995)	27.5	22.6
ODP 659	Tiedemann *et al.* (1994)	22.7	23.3
ODP 677+846	Shackleton *et al.* (1990, 1995a,b)	23.9	25.7
ODP 677	Shackleton *et al.* (1990)	28.6	26.0[b]
Imbrie and Imbrie's model	Imbrie & Imbrie (1980)	58.2	47.6
Summer insolation at 65°N	Laskar *et al.* (1993)	49.2	40.7

[a]Planktonic δ^{18}O record.
[b]Calculated only over the 0–2.6 Myr time interval.

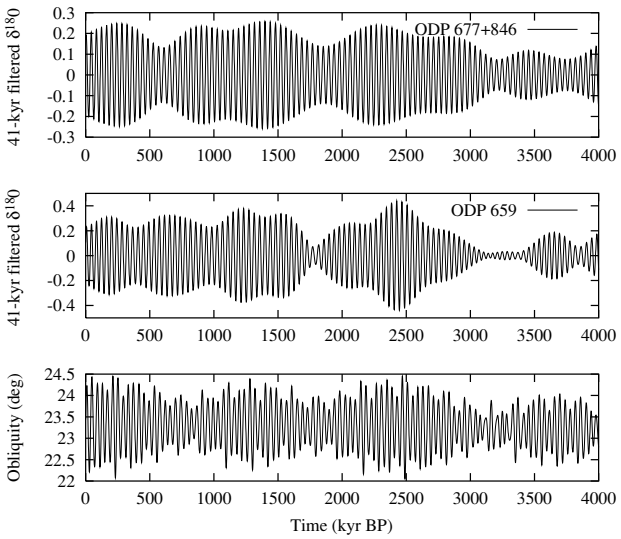

Figure 7. Comparison between the filtered 41 kyr components in the δ^{18}O benthic records of the respective ODP 659 and composite ODP 677+846 and our nominal obliquity solution over the last 4 Myr. The sharp filtering interval includes all the frequencies between 30 and 34 arcsec yr^{-1} (see Table 1). These frequencies contribute to the quasi-totality of the secular obliquity change amplitude (∼90 per cent for the main 41 kyr and the ∼39.6 kyr cycles).

given in Fig. 7 where the high-resolution and astronomically-dated benthic records of the Atlantic ODP Site 659 (Tiedemann *et al.* 1994) and the composite record of the equatorial Pacific ODP Sites 677 and 846 (Shackleton *et al.* 1990, 1995a,b) are filtered in a sharp 41 kyr band and compared to the obliquity over the last 4 Myr. The amplitude modulation of the 41 kyr cyclicity appears quite similar in the astronomical forcing and in the palaeoclimatic records, suggesting a quasi-linear simple relationship in this band, at least before ∼1 Ma. The obliquity-related high-amplitude peaks close to ∼1.2 Ma and ∼2.4 Ma and the amplitude minima close to ∼1.8 Ma and ∼3.1 Ma are well visible in the filtered records, especially for the Site 659, whereas an additional minimum at ∼500 ka is visible in the 677 + 846 composite record. This minimum is, for example, also present in the DSDP Site 607 record (Ruddiman *et al.* 1989).

The modulation produces significant temporal variations of the secular obliquity change. To incorporate the impact of a slow modulation, we approximated at second order the obliquity curve $\varepsilon(t)$ and the previous 41 kyr filtered and here calibrated ice volume response $\Theta(t)$ by the modulation of a single periodic term close to ∼41 kyr cycle so that:

$$\begin{aligned}\varepsilon(t) &= \varepsilon_m(t)\cos(\nu_1 t) + \overline{\varepsilon}\\ \Theta(t) &= \Theta_m(t)\cos(\nu_1 t - \zeta_i) + \overline{\Theta}\end{aligned} \tag{46}$$

where $\Theta_m(t)$ and $\varepsilon_m(t)$ are slow modulating functions of time. In that case, following the same approach used in Section 2, the secular obliquity change, averaged here over an obliquity cycle in (22) and (23), does not affect the slow modulating functions. It results that the 'instantaneous' secular obliquity change (44) is proportional to the product $\Theta_m(t)\ \varepsilon_m(t)$. The secular obliquity change is maximal or minimal during the respective maxima and minima of the obliquity variations only if it also corresponds to the respective maxima and minima of the obliquity-related ice volume response.

In order to display such properties, precession eqs (1) were integrated backward over 3.5 Myr using the glaciation-induced perturbations in the dynamic ellipticity given by (45) adapted to a backward integration. The ice load history is constrained by the benthic composite ODP 677+846 and ODP 659 oxygen-isotopic records. A nominal obliquity solution was also constructed similarly over the last 5 Myr, as discussed in Section 1. By assuming the ice load history, we have not considered the complete feedback loop described in Section 1. Such integrations thus require careful analyses.

Comparison with the theoretical secular obliquity change (44) is possible only if the ice phase lag ζ_i is nearly constant over the integration time scale. The choice of Site 677 and Site 659 records is related to this condition. The age model for the Site 659 was developed by oxygen-isotopic correlation to the δ^{18}O record of ODP Site 677 for the interval 0–2.85 Ma (Tiedemann *et al.* 1994). In turn, the Site 677 δ^{18}O was tuned to the Imbrie and Imbrie ice-volume model (Schackleton *et al.* 1990) which incorporates a constant obliquity phase lag. This yields a close phase lock over 0–3 Myr for Site 659, varying here only between 70 and 80°. The composite benthic ODP 677+846 record consists of the benthic ODP 677 record until 1.8 Ma and of the benthic ODP Site 846 record. Conversely, the age model for the benthic δ^{18}O record of the Site 846 was indirectly determined by the astronomical time scale based on the tuning of the porosity signal of the marine core to the summer insolation (Shackleton *et al.* 1995a). It induces a non-constant phase lag varying around the lower value $\sim 60 \pm 20°$ for the oxygen-isotope signal in the obliquity band.

By changing both the mean dynamic ellipticity and the mean obliquity, the glaciation-induced perturbations affect the frequency of the obliquity variations. As a consequence, this produces a slight increase of the phase lag between the fixed ice volume history and the perturbed obliquity curve. Following eq. (45), precession equations were first integrated over the last 3 Myr, including viscoelastic model B and ice load histories respectively based on the ODP 659 and 677+846 records. The relative oblateness change $\Delta J_2^R / J_2^0$ was fixed to 0.5 per cent. We estimated from variations of the precession rate that glaciation-induced perturbations have induced a mean increase of the obliquity period of about ∼9.7 yr, which corresponds to a temporal shift of about 0.7 kyr over the ∼73 obliquity cycles in the course of 3 Myr, which is consistent with the similar analyses of Mitrovica *et al.* (1997). This shift is not negligible owing the sensitivity of the secular obliquity change to the ice sheet phase lag (See Fig. 4). In order to prevent this drawback, both isotopic records have been recalibrated, incorporating a gradual time shift of 9.7 yr. This drawback does not occur when the complete feedback loop is considered, since the phasing is entirely fixed by the ice sheet-obliquity coupling model (30). Finally, in a backward integration, the obliquity curve is 'lagging' the ice volume and a negative drift is expected. For more clarity, the results are here given with the opposite sign as for the corresponding forward integration from the past.

We plotted the smoothed temporal fluctuations between the perturbated obliquity solution and the nominal solution for each glacial history in Fig. 8. The two glacial histories produce a similar effect on the mean obliquity. A positive secular obliquity drift is well observed but slight variations in the slopes of both curves indicate temporal changes in the secular drift. At 3 Ma, the mean obliquity changed by around ∼0.04° which gives a mean secular change of ∼0.013 deg Myr^{-1}. This value is slightly higher than the previous 0.008–0.011 deg Myr^{-1} values expected for a 70–80° phase lag range and for the obliquity-contributions of the Imbrie and Imbrie model. Here, uncertainties in the minor obliquity-cycle contributions and the

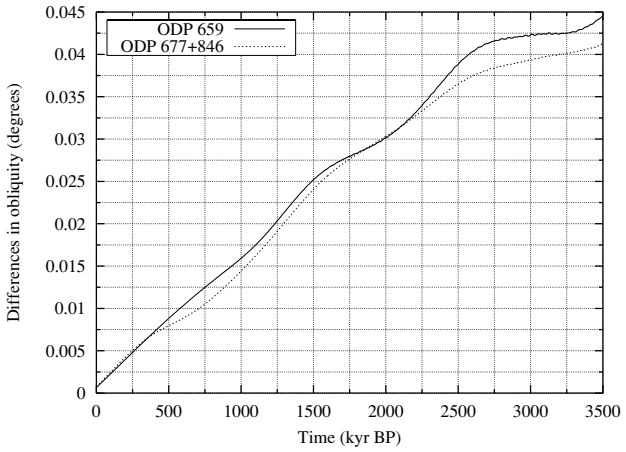

Figure 8. Temporal evolution of the mean obliquity over the last 3.5 Myr induced by both oxygen-isotope records ODP 659 and ODP 677+846 modified ice histories. The temporal fluctuations (in degrees) between the perturbated obliquity solution and the nominal obliquity for the viscoelastic model B were smoothed to remove the short-time scale fluctuations.

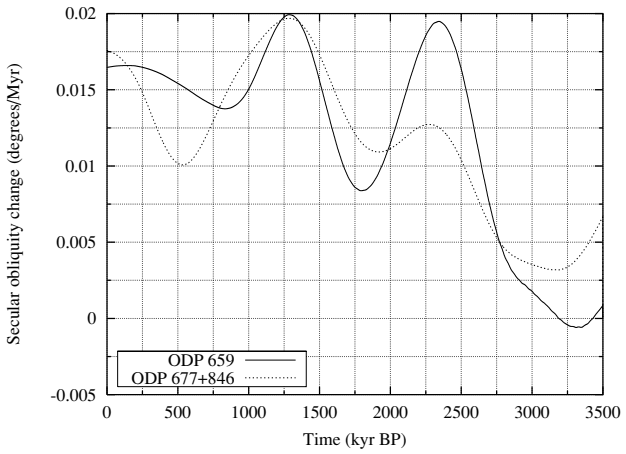

Figure 9. Temporal evolution of the secular obliquity drift over the last 3.5 Myr for both oxygen-isotope records and for the viscoelastic model B. The derivative of the difference between the glaciations-perturbated obliquity solution and the nominal obliquity solution are smoothed to remove the short-time scale fluctuations.

presence of a larger obliquity band in the glacial response can explain this moderate discrepancy. To examine the fluctuations of the secular obliquity drift, we have smoothed the derivative of the difference between the perturbated obliquity solutions and the nominal obliquity solutions over the same 3.5 Myr interval in Fig. 9. For the Site ODP 659, correlative strong minima at 1.7 Ma and 3.2 Ma with the obliquity forcing give strong minima of the secular obliquity change. It becomes negative around 3.2 Ma which is consistent with the large phase fluctuations observed between 3.2 Ma and 3.5 Ma (Tiedemann *et al.* 1994; Clemens 1999). A correlative maximum is also present at 1.3 Ma, when the obliquity is maximal too. The obliquity minimum at ∼0.8 Ma provides the other secular change minimum. For the Site ODP 677+846, some differences are exhibited. Comparable minima are well visible at 1.75 Ma and 3.2 Ma. Before 1.8 Ma, the decrease of the ice phase lag reduces the global secular change and the expected peak at 2.3 Ma is less pronounced. The ice volume response, minimum around 0.55 Ma is also well visible, although more marked as expected. We conclude that the secular obliquity change can undergo large fluctuations (between ∼0 and 0.02 deg Myr^{-1}) related to the obliquity curve modulation and the obliquity-related ice volume response.

4.5 Influence of the lower mantle viscosity

The sensitivity of climate friction to viscosity has been emphasized by Rubincam (1995) with the simple Darwin model. For more realistic layered models, Mitrovica & Forte (1995) and Mitrovica *et al.* (1997) compared the time-dependent perturbations of the dynamical ellipticity with a close ice load history and for a large suite of radial viscosity profiles. They concluded that these variations are unsensitive to the upper-mantle viscosity but are sensitive to the viscosity in the deepest regions of the lower mantle. We have considered lower mantle viscosity values close to 10^{21} Pa s, as required by some postglacial rebound observables. The inversion of data related to the glacial isostatic adjustment does not provide a unique radial viscosity structure and larger lower mantle viscosity values near 10^{22} Pa s, exceeding the upper-mantle viscosity by a factor of 50 to 100, are also suggested (e.g. Nakada & Lambeck 1989), in agreement with independent estimates based on geoid and seismic tomographic data (Forte & Mitrovica 1996). The viscous phase lag ζ_s is closely related to the lower mantle viscosity value. For $\nu_{\mathrm{LM}} \simeq 10^{22}$ Pa s, the surface loading compensation is close to 70 per cent (Mitrovica & Forte 1995) suggesting a viscous phase lag close to 60°. For $\nu_{\mathrm{LM}} > 10^{23}$ Pa s, the isostatic adjustment is reduced to its elastic component ($\zeta_s \longrightarrow 90^\circ$). As the viscoelastic model used in Ito *et al.* (1995), and hence by Williams *et al.* (1998), contains a lower mantle viscosity value of 10^{23} Pa s, they should have found a nearly elastic behaviour, that is clearly not observed. According to eq. (44) and for the single dominant 41 kyr cycle, the secular obliquity change is proportional to the dimensionless quantity

$$H(\zeta_s) = \sin(\zeta_i) - f(\zeta_s)\sin(\zeta_i + \zeta_s). \tag{47}$$

We plotted this function for an ice phase lag $\zeta_i = 74^\circ$ and for the approximation $f(\zeta_s) = 1 - \zeta_s/90^\circ$ in Fig. 10. The previous viscoelastic models A and B are also plotted but are strictly calculated from (36), showing the good agreement with the previous $f(\zeta_s)$ approximation. For the usual range of viscosity $\sim 3.10^{21}$–10^{22} Pa s, the secular change of obliquity may change by a factor 3 or 4, in agreement with the simple Darwin model prediction (Rubincam 1995).

5 APPLICATION TO OTHER GLACIATIONS

In this section, we derive some additional properties and constraints on the climate friction amplitude during the main glacial episodes of the Earth over the last 800 Myr. These episodes are much less documented than the recent glaciations. In particular, the relative change of oblateness largely depends on the location and areal extent of continental ice sheets which are poorly constrained. Moreover, because time limits of the ice ages are so broad (≃50 Myr for each interval), tectonic arrangement and ice distribution may well have changed during each interval. However, both continental and ice distributions were 'chosen' relatively to the available constraints to nearly maximize the relative change of oblateness and thereby the amplitude of the obliquity change.

The higher value of the precession constant in the past due to tidal dissipation in the Earth-Moon system has modified the past main

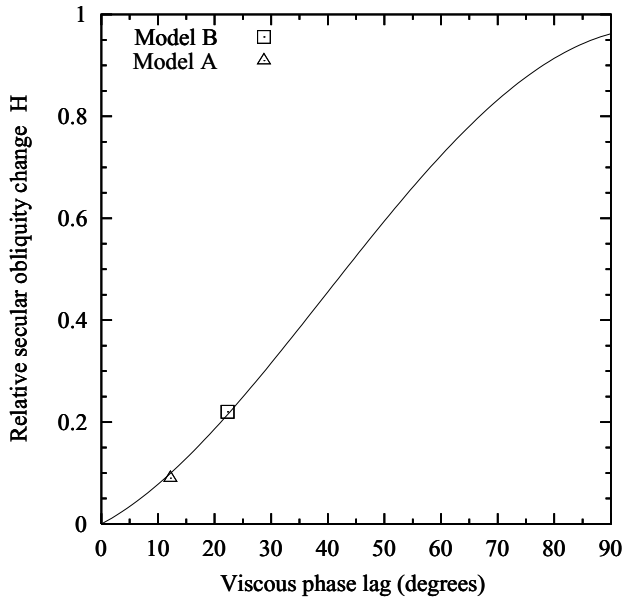

Figure 10. The relative secular drift of obliquity $H(\zeta_s) = \sin(\zeta_i) - f(\zeta_s)(\sin(\zeta_i + \zeta_s)$ as a function of the viscous phase lag ζ_s. The ice sheet lag to obliquity variations is fixed to $\zeta_i = 74^\circ$. Corresponding values for the viscoelastic model A ($\nu_{\rm LM} = 10^{21}$ Pa s) and B ($\nu_{\rm LM} = 3.10^{21}$ Pa s) are also plotted. The viscous phase lag is an increasing function of the lower mantle viscosity.

obliquity frequency $\nu_1 = \overline{\alpha}\cos\overline{\varepsilon} + s_3$ (Berger *et al.* 1992) but this change is affected by the uncertainty of the past tidal dissipation parameter (Néron de Surgy & Laskar 1997). However, for the dominant obliquity cycle, the secular obliquity change can be written from (14) and (44) as:

$$\frac{d\bar{\varepsilon}}{dt} = \frac{\Delta J_2^R}{\overline{J_2}} \frac{a_1\Theta_1}{4} \frac{\nu_1 - s_3}{\nu_1} \left(1 + k_2^{L,E}\right) \times [\sin(\zeta_i) - f(\nu_1)\sin(\zeta_i + \zeta_s(\nu_1))] \quad (48)$$

which is only slightly affected by moderate changes in ν_1. We assume that the past mean Earth oblateness $\bar{J}_2$ is proportional to the square of the angular velocity (ω^2) as for a planet in hydrostatic equilibrium (e.g. Lambeck 1980).

5.1 Permo-Carboniferous glaciations (∼340–260 Ma)

Geological evidence of massive glaciations during the Permo-Carboniferous period when glaciers probably reached sea level around the margins of a Gondwanan supercontinent approximately centred on the South Pole are documented (e.g. Crowell 1999). Glaciations lasted over ∼80 Myr with a peak extent around ∼60 Myr. Although glacial data have been recorded on all Gondwanan continents, the maximum ice spread is still poorly constrained and we refer to the glacial reconstructions of Crowley & Baum (1991) which reflect the possible ranges of ice cover as available from geological data. Concurrently, the investigation of eustatic sea level variations documented in sedimentary sequences (cyclothems) of North America and Europe (Ross & Ross 1985; Heckel 1986; Maynard & Leeder 1992) suggest that cyclical glacial–interglacial fluctuations could have accounted for ranges in sea level changes between 100 and 200 m (Maynard & Leeder 1992). Although the timing of the sea level curves is uncertain, Heckel (1986) found that these fluctuations have a major periodicity close to the 400 kyr eccentricity cycle and minor cycles close to the obliquity and ∼100 kyr eccentricity periods. The presence of Milankovitch cycles is also suggested by climate model simulations (Crowley *et al.* 1993).

Assuming the conservation of the water/ice mass and a present land/sea ratio, a maximal eustatic sea level change of 200 m provides an upper value of the total ice mass $M_i \sim 7.10^{19}$ kg exchanged during glacial–interglacial cycles. This latter value is close to the lower estimate of the extreme ICE III glacial scenario of Crowley & Baum (1991).

Assuming that the ICE III ice extent can be approximated by a single ice cap from South Pole to $\theta_0 = 50^\circ$S covering a very large part of the Gondwanan supercontinent, the complete melting of this ice cap into the global ocean yields to an approximate relative change of oblateness (Thomson 1990) of

$$\frac{\Delta J_2^R}{\overline{J_2}} = \frac{M_i}{M_e} \frac{\cos(\pi/2 - \theta_0)}{\overline{J_2}} \simeq 0.8 \text{ per cent} \quad (49)$$

for a length of day equal to 0.95 times the present value. This value is probably an overestimate since a more accurate determination of the spread and timing of ice accumulation suggests that the whole of Gondwana was probably never glaciated at the same time (Roberts 1976; Veevers *et al.* 1994). Furthermore, the rifting of the supercontinent from the South pole during Permo-Carboniferous period has significantly reduced the polar symmetry of the continental ice sheets and hence the oblateness change.

The apparent predominance of 400 kyr and 100 kyr eccentricity-presumed cycles suggests that the obliquity contribution Θ_1 could have not exceeded the Plio-Pleistocene value of 25 per cent. With a rigid-Earth oblateness change of 0.8 per cent, a maximal obliquity contribution of 25 per cent and a main obliquity period of ∼35.0 kyr, the secular obliquity drift is given by Fig. 4 but with a lower amplitude due to a reduced obliquity contribution with respect to the Imbrie and Imbrie model. The maximal positive secular change does not exceed ∼0.02 deg Myr^{-1} for the viscoelastic model B. The maximal negative drift is obtained for $\zeta_i = 0^\circ$ and is very close to −0.02 deg Myr^{-1}. This provides a maximal obliquity change value of ± ∼1.2° during the ∼60 Myr duration of maximal glacial extent.

5.2 Neoproterozoic glaciations (∼750 ± 200 Myr)

Although their dating is uncertain, two broad intervals of widespread glaciations are well documented: the Sturtian glaciation (∼750–700 Ma) and the Varanger glaciation (∼620–570 Ma) (e.g. Kennedy *et al.* 1998; Crowell 1999; Evans 2000). The labels Sturtian and Varanger are commonly used over the whole Earth, but a worldwide correlation is very premature, since the present large uncertainties in age dating of, and lithostratigraphic relationships between glacial deposits of each interval, leave open the possibility that glaciations are diachronous (e.g. Kröner 1977; Crowell 1999). For both glacial intervals, we assumed that the length of the day was close to the ∼650 Ma value of 21.9 hr (Williams 1993).

5.2.1 Sturtian glacial interval (∼750–700 Ma)

Although palaeoreconstructions for the Sturtian interval (∼750–700 Ma) are still uncertain, the presence of a supercontinent named 'Rodinia' centred around the equator is largely admitted at the beginning of the Sturtian interval (ca. 750 Ma) (Torsvik *et al.* 1996; Dalziel 1997; Weil *et al.* 1998; Meert 2001). This supercontinent can be modelled by a spherical continental element situated between the latitude 40°N–40°S and with a $\Delta\phi = 170^\circ$ longitude extension

which preserves the present land-sea repartition. In this context, the non-identification of a high-latitude glacial deposit may be a simple consequence of the lack of polar continents.

To get an idea of the probable maximal change of oblateness, and to take account of possible widespread continental glaciations, we assumed that the whole supercontinent was entirely covered by an uniform ice sheet of 3.5 km thickness which can uniformly melt in the complementary ocean. The resulting change of the polar inertia arises from both ice and ocean contributions:

$$\Delta C^R = \Delta C_{\rm ice} + \Delta C_{\rm ocean}. \tag{50}$$

During a deglaciation process, subtracting ice from the continents yields a negative ice-component inertia contribution, which is here

$$\Delta C_{\rm ice} = -M_i R^2 \left(1 - \frac{1}{3}\cos^2\theta_0\right), \tag{51}$$

where M_i is the total water/ice mass exchanged and $\theta_0 = 50^\circ = 90^\circ$–$40^\circ$ the minimal co-latitude of the ice distribution. In contrast, the uniform increase of global sea level yields a positive ocean inertia contribution

$$\Delta C_{\rm ocean} = M_i R^2 \left[\frac{4\pi/3 - \Delta\phi\left(\cos\theta_0 - 1/3\cos^3\theta_0\right)}{2\pi - \Delta\phi\cos\theta_0}\right]. \tag{52}$$

As our ice distribution corresponds to a total water/ice mass M_i of $\sim 4.8 \times 10^{20}$ kg, from (29), (51) and (52), it results a relative oblateness change of $\Delta J_2^R/\overline{J_2} \simeq -2.6$ per cent which, as expected for predominantly low-latitudes glaciations, is a high negative value.

However, the influence of the obliquity on the direct summer insolation forcing significantly decreases at latitudes lower than $\pm 60^\circ$. In tropical zones, the insolation forcing and the climate response are nearly entirely dominated by the climatic precession signal (with present $\sim$23 and 19 kyr dominant cycles). An ice volume signal derived from the truncation or rectification of the summer insolation at low-latitudes will thus contain a negligible obliquity signal. Moreover, for high latitude glaciations, the ice sheets sensitivity to the summer insolation corresponds to the correlative timing of the yearly maximum temperature while in equatorial land areas, two seasonal temperature peaks occur at both equinoxes. It is then unclear how the accumulation/sublimation processes of equatorial sea level glaciers would work. Crowley *et al.* (1992) used an energy-balance model to compute the time-series of the yearly maximum temperature which is a composite of a primary autumnal equinox signal and a secondary vernal equinox signal. They showed that they are similar to a rectification of a low-latitude insolation signal, resulting in power arising at eccentricity periods. They also suggested that this process could be amplified in a supercontinental configuration. We conclude that the obliquity change due to climate friction should have been negligible during the Sturtian interval. An additional important consequence is that a high-obliquity hypothesis ($>54^\circ$) (Williams 1975, 1993) which also predicts a preponderance of low latitude glacial deposits, is conflicting with an efficient climate friction mechanism.

5.2.2 Varanger glacial interval (∼620–570 Ma)

5.2.2.1 Boundary conditions. There is considerable support for a convergence of most of the continental landmasses near the South polar region during the Varanger glaciation (Torsvik *et al.* 1996; Dalziel 1997; Meert 2001). This convergence could have been included in a transient global supercontinent named 'Pannotia' (Dalziel 1997). We have modelled the continental distribution at the end of the Varanger interval ($\sim$580 Ma) by a spherical cap of maximal colatitude $\theta_0 = 60^\circ$S and an additional spherical element situated between the latitude 30°S–30°N (including Australia, India and Antarctica) with a longitude extension $\Delta\phi = 40^\circ$ in order to preserve the present land-sea repartition (though palaeoreconstructions suggest a lower continental/ocean ratio than today). As the continental distribution permits predominantly mid to high-latitude glaciations that favour the climate friction effect, this glacial interval was investigated in detail. To estimate and maximize the possible oblateness change in absence of glacial constraints, we consider the simplest case of a spherical cap of uniform thickness h and co-latitude (or angular radius) θ in a spherical coordinate system with the South polar axis centred on the ice cap. If $\theta < \theta_0$, the complete and synchronous melting of the ice cap of mass M_i gives a negative polar inertia contribution

$$\Delta C_{\rm ice} = -\frac{M_i R^2}{3}(2 - \cos\theta - \cos^2\theta) \tag{53}$$

where $M_i = \rho_i h \times 2\pi R^2 (1 - \cos\theta)$ and where ρ_i is the ice density. When $\theta > \theta_0$, the ice cap incorporates the low-latitude glaciations of the equatorial landmass and the polar inertia becomes

$$\Delta C_{\rm ice} = -M_i R^2 \left(\left[\frac{4\pi/3 + (\Delta\phi - 2\pi)\left(\cos\theta_0 - 1/3\cos^3\theta_0\right)}{2\pi(1 - \cos\theta_0) + \Delta\phi(\cos\theta_0 - \cos\theta)}\right] + \left[\frac{\Delta\phi(1/3\cos^3\theta - \cos\theta)}{2\pi(1 - \cos\theta_0) + \Delta\phi(\cos\theta_0 - \cos\theta)}\right]\right) \tag{54}$$

where $M_i = \rho_i h \times R^2[2\pi(1 - \cos(\theta_0)) + \Delta\phi(\cos(\theta_0) - \cos(\theta))]$. In both cases, assuming a uniform increase of the global ocean outside the continental distribution and the conservation of the water/ice mass, the ocean polar inertia change is

$$\Delta C_{\rm ocean} = M_i R^2 \left[\frac{4\pi/3 + 2(\pi - \Delta\phi)\left(\cos\theta_0 - 1/3\cos^3\theta_0\right)}{2\pi(1 - \cos\theta_0) + 2(2\pi - \Delta\phi)\cos\theta_0}\right]. \tag{55}$$

The relative oblateness change $\Delta J_2^R/\overline{J_2}$, obtained from (29), is shown in Fig. 11 as a function of the angular extent of the cap and for a uniform ice thickness of 3 and 3.5 km. In comparison, palaeotopographic reconstructions at the LGM suggest that the main ice sheets (Antarctica, Greenland or Laurentia) had an equivalent thickness (volume/area) of less than 2.5 km (Tushingham & Peltier 1991;

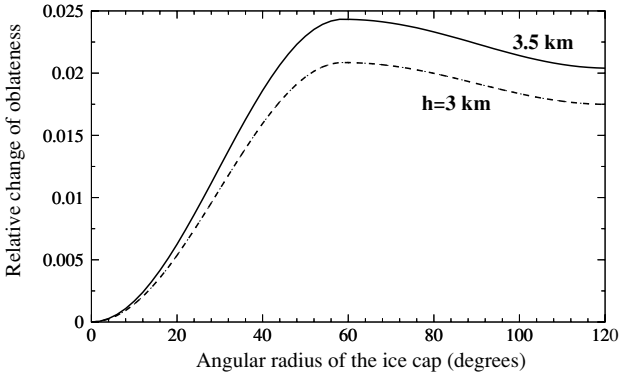

Figure 11. Relative change of oblateness $\Delta J_2^R/\overline{J_2}$ for a spherical ice cap centred on the South Pole, as a function of its angular radius, corresponding to the co-latitude of its maximal extent, and for an uniform thickness of 3 km (dashed line) or 3.5 km (solid line). The modelized continental palaeogeography corresponds to the end of the Varanger interval ($\sim$580 Ma). The maximal angular radius is thus 120°.

Peltier 1994). For both thicknesses, the oblateness change increases with the size of the cap (and θ) up to a maximum for an angular radius of $\theta \sim 60^\circ$. Indeed, when θ increases, the global ice mass increases but it corresponds to lower latitudinal locations closer to the equatorial inertia axis. In the absence of any constraints on the cap thickness, we cannot rule out that larger thicknesses and global ice quantities than at the LGM were present, but it does not necessarily imply that larger ice volumes were transported during glacial cycles. To maximize the oblateness change and to take into account of low-latitudes glaciations, we choose here a maximal oblateness change of 2 per cent, corresponding to a complete continental ice covering with a 3.5 km ice thickness. It also corresponds to the maximal value for a 3 km thickness. In the former case, it corresponds to a total ice mass of 4.8×10^{20} kg which is entirely and synchronously removed. It should be noted that this is about one order of magnitude higher than the water/ice mass exchanged during the last deglaciation cycle. Williams *et al.* (1998) proposed a maximal 2.6 per cent value but without equatorial landmasses.

5.2.2.2 Influence of non-linearities. As noted in Section 3, the possible increase in the ice sheet size may lead to an increase in the non-linear response of ice sheets to insolation forcing, that affects the obliquity contribution to glacial variability. For that purpose, we created a set of ice-volume models derived from the non-linear one of Imbrie & Imbrie (1980). Assuming that the characteristic ice time response T_m is proportional to $V^{1/5}$ (Bahr *et al.* 1998), the change by a factor of 10 to the global ice volume here yields a new value of T_m close to $17 \times (10)^{1/5} \simeq 30$ kyr. We considered increasing values of the non-linearity coefficient b, and hence of the time constant ratio τ_A/τ_M, ranging from 0.6 to 0.9. The ice volume models were computed over 5 Myr and we estimated the main obliquity-cycle contribution over that time interval in Table 4 as for the Table 3. Each model includes a present initial obliquity and a forcing summer insolation at 65°N. As we considered the complete growth and ablation of the ice cap, the calibration (See eq. 28) was made, for each integration, between the maximal and the minimal value of the ice volume evolution over 5 Myr. For the nominal Imbrie and Imbrie model described in Section 3, the obliquity contribution becomes ∼20.5 per cent (it means that the maximal amplitude of this ice volume history is about twice as long than the last deglaciation cycle amplitude), a value close to the mean value extracted from oxygen-isotope records. The correlative decrease of the main obliquity cycle contribution with b illustrates the transfer of the ice-volume variability to higher periodicities of the eccentricity band. For our maximal value $b = 0.9$, the obliquity contribution is divided by a factor ∼2. We also found that the 400 kyr and/or 100 kyr cycles dominate each ice volume signal, that we believe to be more compatible with the complete waxing and waning of a 4.8×10^{20} kg ice mass.

5.2.2.3 Numerical simulations. We simulated the possible secular obliquity change during the Varanger interval for three different models. Each model contains a constant $\tau_A/\tau_M = 4$ ratio value.

(1) The first model, identical to the nominal model used for Plio-Pleistocene glaciations, includes an initial present obliquity and a forcing summer insolation at 65°N, giving an obliquity contribution of ∼20 per cent with the new calibration. As shown in Table 4, this obliquity contribution value represents the maximal possible value and lower obliquity contributions are probably more realistic regarding to the huge ice cap here considered.

(2) In the second model, as most of the ice distribution may extend to lower latitudes than Quaternary (here 30°), the summer insolation at 30°N was used as the reference forcing insolation. We found that the obliquity contribution dramatically falls to ∼4 per cent in the ice volume signal.

(3) For the third model, in order to compare with the G. E. Williams (1993) scenario, a high initial obliquity of 55° and a forcing summer insolation at 65°N is included. It corresponds to a 62.8 kyr main obliquity period and to a close to 20.0 per cent obliquity contribution.

Note that the use of summer insolations at corresponding southern latitudes would provide identical results due to the very small Earth's eccentricity. In a second step, for each of the previous models, the values of τ_A and τ_M have been changed to get the maximal range of the ice phase lag allowed by the Imbrie and Imbrie model (i.e. 0–90°). However, the ratio τ_A/τ_M must be kept constant to maintain a nearly constant obliquity contribution of respectively 20, 4 and 20 per cent for the three models previously described. Precession equations were integrated over 5 Myr as in Section 4 for each set of models and with a positive relative change of oblateness of 2 per cent. The secular obliquity changes obtained are shown in Fig. 12. The results are in very good agreement with the theoretical and numerical experiments previously summarized in Figs 4

Table 4. Obliquity contribution values Θ_1 for several non-linear ice volume responses based on the Imbrie & Imbrie (1980) model. For each model, $T_m = 30$ kyr. The non-linearity parameter b controls the accumulation/melting time ratio τ_A/τ_M (eq. 31) and thereby the degree of the non-linear response. The forcing insolation is the summer insolation at 65°N.

Non-linearity parameter b	Ratio τ_A/τ_M	Obliquity contribution Θ_1 (per cent)
0.6	4.0	19.8
2/3	5.0	17.6
0.7	5.7	16.7
0.75	7.0	14.1
0.8	9.0	12.4
0.9	19.0	9.2

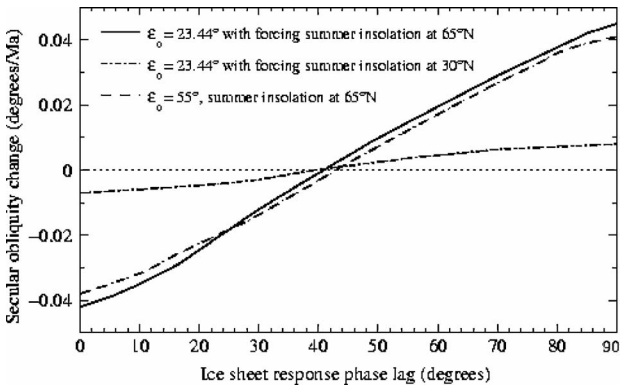

Figure 12. Summary of the secular obliquity drifts obtained by numerical integrations of the precession equations over 5 Myr and simulating an extreme Varanger glacial episode as a function of the ice sheet lag to main obliquity cycle forcing. All the runs include a rigid-Earth oblateness change $\Delta J_2^R/\bar{J}_2^0 = 2$ per cent, the viscoelastic model B and ice volume models derived from Imbrie & Imbrie (1980). The solid line corresponds to a summer insolation forcing at 65° and a present initial obliquity $\varepsilon_0 \simeq 23.44^\circ$ (The main obliquity cycle is thus ∼ 30.7 kyr). The dashed-dotted line corresponds to a summer insolation forcing at 30°N and a present initial obliquity. The dashed line is for an initial obliquity at 55° and a summer insolation forcing at 65°N. The obliquity contribution is respectively 20, 4 and 20 per cent for each model.

and 6 for different obliquity contribution values. For the three models, the secular obliquity changes vanish for $\zeta_i \sim 40^\circ$ and are only weakly affected by the change of initial obliquity. A subsequent higher obliquity period corresponds to a lower viscous phase lag shifting the secular obliquity change curve to the right, but with a nearly similar global amplitude (see eq. 48). For a summer insolation forcing at high latitudes, the maximal negative drift is ~ -0.04 deg Myr^{-1}, but obtained for $\zeta_i = 0^\circ$. The possible maximal drift is close to $\sim$0.045 deg Myr^{-1} in the 0–90° ice phase lag range but may reach the maximal value $\sim$0.06 deg Myr^{-1} for $\zeta_i = 133^\circ$ (see Fig. 4 for the extension $\zeta_i > 90^\circ$). With a summer insolation forcing at 30°N, the secular drift is lower than $\pm$0.01 deg Myr^{-1}, which is similar to the Pleistocene value, and in good agreement with the theoretical rate for a 4 per cent obliquity contribution. A forcing summer insolation at 45°N, as used by Williams *et al.* (1998), would thus give an intermediary maximal rate close to $\pm$0.02 deg Myr^{-1}, fifteen times smaller than their average -0.3 deg Myr^{-1} value. In any case, if we assume hypothetical, continuous and extreme glaciation–deglaciation cycles during the approximative maximal $\sim$50 Myr duration of the Varanger interval, the obliquity changes obtained are lower than 2° for the current range $0 < \zeta_i < 90^\circ$.

5.3 Discussion

Our simulations for the Varanger glacial interval assume a large oblateness change of 2 per cent, that is probably an overestimate. The synchronous, periodic and complete melting of a $\sim 4.8 \times 10^{20}$ kg ice mass would yield drastic changes of eustatic sea level of more than 1 km, which probably should be preserved in the stratigraphic records. Changes of the order of hundred of metres in eustatic sea level (>160 m), comparable to maximal Permo-Carboniferous values are documented during the Neoproterozoic (Christie-Blick *et al.* 1999) but some of them have been attributed to local tectonic mobility (Christie-Blick *et al.* 1990). However, sea level change estimate caused by their periodic partial or complete waxing and waning are still not available. Additionally, large eustatic-sea level changes of more than 1 km would lead to large coastal inundations, significantly decreasing the global change of oblateness. Williams *et al.* (1998) proposed that a constant 2.6 per cent value could have existed during a 100 Myr interval between $\sim$600 and 500 Ma, but such huge and long glaciations are not documented (e.g. Crowell 1999). The rifting of the Laurentia landmass from the South Pole towards low latitudes, which induces a major reduction of the polar continentality, is well constrained around $\sim$570 Ma (McCausland & Hodych 1998). This also suggests that the proposed $\sim$2 per cent maximal value may be valid only during the likely maximal continental polar clustering at the end of the Varanger glacial interval.

Our ice distribution as in Williams *et al.* (1998) requires a preponderance of high-latitude glacial deposits. This hypothesis is at odds with a high initial obliquity hypothesis. High obliquity greatly amplifies seasonality, especially in the polar areas, creating cold winters, but very hot summers with maximal melting, thus preventing high-latitude ice accumulation according to the Milankovitch theory. Our ice extent is then more compatible with a current (or even lower) initial obliquity. There is still no current consensus on the extent and the timing of the Neoproterozoic glaciations and most of the controversy is mainly centred on the interpretation of palaeomagnetic measurements and criteria, which are beyond the scope of this paper. A recent review of Meert & Van der Voo (1994) suggested that glaciations had been confined to latitudes higher than 25°, while Evans (2000) found no reliable and convincing high-latitude glacial deposits. In any case, the proof of a single and reliable high-latitude deposit would be one way to undermine a past high-obliquity scenario. To account for the paradoxical low-latitude glaciations, Hoffman *et al.* (1998) proposed a global synchronous refrigeration of the Earth with the entire oceans frozen over perhaps 10 Myr as a result of a runaway albedo feedback. They argued that the drastic reduction of snowfall and of the hydrological cycle leads to the rapid ablation of land-based ice sheets, creating a thin continental ice cover. In this scenario, the sensitivity of a such ice distribution to changes in orbital and axial parameters is unclear. It is likely that the presence of thin continental ice sheets may produce only reduced oblateness changes, but the occurrence of glacial–interglacial conditions, that seem rather problematic, requires further investigation.

It appears that the negative drift of -0.3 deg Myr^{-1} proposed by D.M Williams *et al.* (1998) and arguing in favour of the G.E. William's high obliquity scenario, is one and may be two order of magnitude larger than the maximal possible rate found here ($\pm$0.04 deg Myr^{-1}) and abnormal parameters are required to establish agreement between the inferred and predicted rates. Even with an important lower mantle viscosity close to 10^{22} Pa s, the maximal obliquity change is lower than 10° during the Varanger interval. A negative decrease of the obliquity is expected for only extreme (and probably unrealistic) values of the ice phase lag ($\zeta_i \gg 224^\circ$). The case $\zeta_i < 44^\circ$ seems more realistic but it provides a significant secular obliquity change only for $\zeta_i \simeq 0^\circ$. Hence, the climate friction effect is unlikely to have been an important factor in modifying the Earth's obliquity during the Neoproterozoic glaciations.

We have summarized the maximal obliquity change due to climate friction during the four main glacial periods examined here in Table 5. The maximal possible global obliquity change proposed for the last 800 Myr of Earth's glaciations thus ranges only between $\pm$3 and 4° for a current lower mantle viscosity value.

We obtained these values using the presently available models and parameters, but it is certain that some improvement is still welcome. The knowledge of the orbital and rotational part of the problem is very mature, and we do not expect much advance in this direction. This is not fully the case for the understanding of the viscoelastic structure of the Earth and thus of its response to the ice load over

Table 5. Maximal indicative obliquity changes during the recent main Earth' s glacial periods. Duration and synchronicity of glacial deposits for Neoproterozoic glacial intervals are very uncertain.

Ice-age	Period (BP)	Duration	Maximal obliquity change (°)
Late Pliocene-Pleistocene[a]	$\sim$0–3 Ma	$\sim$3 Myr	$\sim 0.04^\circ$
Permo-Carboniferous	$\sim$270–330 Ma	$\sim$60 Myr	$< \pm 1.2^\circ$
Varanger glacial interval	$\sim$570–620 Ma	$\sim$50 Myr	$< \pm 2^\circ$
Sturtian glacial interval	$\sim$700–750 Ma	$\sim$50 Myr	$\sim 0^\circ$(?)[b]

[a]If we extend to the whole Late Cenozoic ice-age of duration $\sim$40 Myr with the current rate 0.01 deg Myr^{-1}, the maximal change on this interval is likely less than $\sim 0.4^\circ$ due to smaller Pre-Pliocene glaciations.
[b]Assuming only low-latitude glaciations allowed by the continental distribution.

long period of times. The less constrained aspect of the present work is certainly the glacial history of the Earth over the considered geological periods, both through the climate response to the insolation forcing, or directly through geological data and palaeogeographic reconstitutions. Nevertheless, despite these uncertainties that have been largely taken into account in our study, we consider that the secular obliquity changes estimated in Table 5 represent upper values.

6 CONCLUSION

We have re-estimated the change of the Earth's obliquity due to obliquity–oblateness feedback during the Earth's recent major glacial episodes, comparing theoretical and numerical formulations. Previous works of Ito *et al.* (1995) and Williams *et al.* (1998) have considered that the obliquity variations were the only ice-age driver, whereas only the obliquity contribution to glacial variability plays a role in the feedback resonance process. This has led to significant overestimates of possible obliquity changes. Based on the analysis of high-resolution benthic δ^{18}O records, we found an average secular obliquity change of only $\sim$0.01 deg Myr^{-1} modulated by the amplitude of both the obliquity variation and the ice volume variation in the obliquity band, during the recent Plio-Pleistocene glaciations. Having also examined the possible constraints on the climate friction amplitude, we are led to three main conclusions:

(1) The progressive intensification of the glacial cycle amplitude since the onset of the Northern Hemisphere glaciations ($\sim$3 Ma) and at the Mid-Pleistocene transition ($\sim$800 ka) does not document a correlative increase of the obliquity-driven ice volume but suggests a quasi-linear relationship between obliquity variations and obliquity-related ice volume variations. This suggests that obliquity variations may not remove more ice/water material than during the recent glaciations and thus provide a strong global limitation to climate friction phenomena. There is, unfortunately, no sufficiently accurate data during Pre-Cenozoic glaciations to investigate this property.

(2) A possible global extension of the ice distribution to lower latitudes probably increases the non-linearities in the ice volume response to insolation forcing and the correlative transfer to longer Milankovitch periodicities (probably eccentricity) and thus decreases the obliquity contribution to glacial variability.

(3) The lower latitudinal ice extension may induce a lower latitudinal insolation forcing which contains a weaker obliquity contribution. In the extreme case of predominantly low-latitude glaciations, the secular obliquity change would probably be negligible.

It results in the paradoxical idea that the climate friction effect is not increasing with the amplitude of the ice-age as was previously assumed. Even when these constraints are minimized, we found that the obliquity change has probably not exceeded $\pm \sim 2^\circ$ during the Neoproterozoic glacial intervals in disagreement with the previous work of Williams *et al.* (1998), and that reasonable ice phase lags lead, in fact, to an increase of the Earth's obliquity, as suggested by Rubincam (1995). We also show that the high obliquity scenario as proposed by Williams (1975, 1993) is in contradiction with an efficient climate friction mechanism, as low-latitude glacial cycles are most probably not driven by obliquity, but by eccentricity and climatic-precession variations. We thus find that climate friction cannot explain the rapid 30° decrease of the obliquity at the Late Precambrian–Cambrian boundary proposed by G.E. Williams (1975, 1993). In his initial scenario, G.E. Williams (1993) suggested that core–mantle friction could have explained this substantial obliquity decrease. But it was demonstrated by Néron de Surgy & Laskar (1997), and confirmed by Pais *et al.* (1999), that it not only requires abnormal values of core viscosity but, due to the conservation of the normal component of the angular momentum, it is also conflicting with the palaeorotation data. We are thus led to conclude that until some new mechanism is proposed, the high obliquity scenario must be rejected as a possible explanation of the observed low latitude glaciations of the Neoproterozoic.

ACKNOWLEDGMENTS

The authors thank Alexandre Correia, Yannick Donnadieu, Anne Nédelec and Gilles Ramstein for helpful discussions, M. Gastineau for computational assistance and Heiko Pälike for careful reading of the manuscript. Thanks are also due to J. Imbrie, A. Mix, N. J. Shackleton and R. Tiedemann for making their oxygen-isotope data available. These data are archived at the World Data Center-A for Palaeoclimatology on the web site: www.ngdc.noaa.gov. This work was supported by the PNP and ECLIPSE programmes of CNRS.

REFERENCES

Bahr, D.B., Pfeffer, W.T., Sassolas, C. & Meier, M.F., 1998. Response time of glaciers as a function of size and mass balance: theory, *J. geophys. Res.,* **103,** 9777–9782.

Berger, A., Loutre, M.F. & Laskar J., 1992. Stability of the astronomical frequencies over the Earth's history for paleoclimate studies, *Science,* **255,** 560–565.

Bills, B.G., 1994. Obliquity–oblateness feedback: Are climatically sensitive values of obliquity dynamically unstable?, *Geophys. Res. Lett.,* **21,** 177–180.

Bills, B.G., 1999. Obliquity–oblateness feedback on Mars, *J. geophys. Res.,* **104,** 30 773–30 797.

Chappell, J. & Shackleton, N.J., 1986. Oxygen isotopes and sea level, *Nature,* **324,** 137–148.

Christie-Blick, N., Von der Borch, C.C. & DiBona, P.A., 1990. Working hypotheses for the origin of the Woka Canyons (Neoproterozoic), South Australia, *Am. J. Sci.,* **290,** 295–332.

Christie-Blick, N., Sohl, L.E. & Kennedy, M.J., 1999. Considering a Neoproterozoic Snowball Earth, *Science,* **284,** 1087–1088.

Clemens, S.C., 1999. An astronomical tuning strategy for Pliocene sections: implications for global-scale correlation and phase relationships, *Phil. Trans. R. Soc. Lond.,* A, **357,** 1949–1973.

Correia, A.M., Laskar, J., Néron de Surgy, O., 2003a. Long term evolution of the spin of Venus-I. Theory, *Icarus,* **163,** 1–23.

Correia, A.M. & Laskar, J., 2003b. Long term evolution of the spin of Venus-II.Numerical simulations, *Icarus,* **163,** 24–45.

Crowell, J.C., 1999. Pre-Mesozoic Ice ages: Their bearing on understanding the climate system, *Geol. Soc. Am. Memoir,* **192,** Geological Society of America, Boulder, Colorado.

Crowley, T.J. & Baum, S.K., 1991. Estimating Carboniferous sea-level fluctuations from Gondwana ice extent, *Geology,* **19,** 975–977.

Crowley, T.J., Kim, K.G., Mengel, J.G. & Short, D.A., 1992. Modeling 100 000 year climate fluctuations in Pre-Pleistocene time series, *Science,* **255,** 705–708.

Crowley, T.J., Yip, K.-J.J. & Baum, S.K., 1993. Milankovitch cycles and Carboniferous climate., *Geophys. Res. Lett.,* **20,** 1175–1178.

Dalziel, I.W.D, 1997. Neoproterozoic-Paleozoic geography and tectonics. Review, hypothesis, environmental speculation, *Geol. Soc. Am. Bull.,* **109,** 16–42.

Denton, G.E. & Hughes, T.H., 1981. The Last Great Ice Sheet, *Wiley-Interscience,* New York.

Evans, D.A.D., 2000. Stratigraphic, geochronological, and paleomagnetic constraints upon the Neoproterozoic climatic paradox, *Am. J. Sci.,* **300,** 347–433.

Forte, A.M. & Mitrovica, J.X., 1996. A new inference of mantle viscosity based on a joint inversion of post-glacial rebound and long-wavelength geoid anomalies, *Geophys. Res. Lett.,* **23,** 1147–1150.

Gallée, H., Van Ypersele, J.P., Fichefet, T., Marsiat, C., Tricot, C. & Berger, A., 1992. Simulation of the last glacial cycle by a coupled, sectorially averaged climate-ice sheet coupling, *J. geophys. Res.,* **97,** 15 713–15 740.

Gilbert, F. & Dziewonski, F., 1975. An application of normal mode theory to the retrieval of structural parameters source mechanisms from seismic spectra, *Phil. Trans. R. Soc.,* A, **287,** 545–594.

Harland, W.B., 1964. Critical evidence for a great InfraCambrian glaciation, *Geol. Rund.,* **54,** 45–61.

Hays, J.D., Imbrie, J. & Shackleton, N.J., 1976. Variations of the Earth's Orbit: Pacemaker of the ice ages, *Science,* **194,** 1121–1132.

Heckel, P.H., 1986. Sea-level curve for Pennsylvanian eustatic marine transgression-regressive depositional cycles along midcontinent outcrop belt, North America, *Geology,* **14,** 330–334.

Hilgen, F.J., Lourens, L.J., Berger, A. & Loutre, M.F., 1993. Evaluation of the astronomically calibrated time scale for the Late Piocene and the earliest Pleistocene, *Paleoceanography,* **8,** 549–565.

Hoffman, P.F. & Schrag, D.P., 2002. The snowball Earth hypothesis: testing the limits of global change, *Terra Nova,* **14,** 129–155.

Hoffman, P.F., Kaufman, A.J., Halverson, G.P. & Schrag, D.P., 1998. A Neoproterozoic Snowball Earth, *Science,* **281,** 1342–1346.

Imbrie, J. & Imbrie, J.Z., 1980. Modeling the climatic response to orbital variations, *Science,* **207,** 943–953.

Imbrie, J. *et al.,* 1984. The orbital theory of Pleistocene climate: support from a revised chronology of the marine δ^{18}O record, in *Milankovitch and Climate*, pp. 265–305, eds Berger, A., Imbrie, J., Hays, J., Kukla, G. & Salztmann, B., Reidel, Dordrecht, Netherlands.

Imbrie, J. *et al.,* 1992. On the structure and origin of major glaciation cycles: 1. Linear responses to Milankovitch forcing, *Paleoceanography,* **7,** 701–738.

Imbrie, J. *et al.,* 1993. On the structure and origin of major glaciation cycles: 2. The 100 000 year cycle, *Paleoceanography,* **8,** 699–735.

Ito, T., Masuda, K. & Matsui, T., 1995. Climate friction: A possible cause for secular drift of Earth's obliquity, *J. geophys. Res.,* **100,** 15 147–15 161.

Jiang, X. & Peltier, W.R, 1996. Ten million year histories of obliquity and precession: the influence of the ice-age cycle, *Earth planet. Sci. Lett.,* **139,** 17–32.

Kennedy, M.J., Runnegar, B., Prave, A.R., Hoffman, K.H. & Arthur, M.A., 1998. Two or four Neoproterozoic glaciations?, *Geology,* **36,** 1059–1063.

Kinoshita, H., 1977. Theory of rotation of the rigid Earth, *Celest. Mech.,* **15,** 277–326.

Kirschvink, J.L., 1992. Late Proterozoic low-latitude global glaciation: The snowball Earth, in *The Proterozoic Biosphere: A Multidisciplinary Study,* pp. 51–52, eds Schopf, J.W. & Klein, C., Cambridge University Press, Cambridge.

Knoll, A.H. & Walter, M.R., 1992. Latest Neoproterozoic stratigraphy and Earth history, *Nature,* **356,** 673–678.

Kröner, A., 1977. Non-synchroneity of Late Precambrian glaciations in Africa, *J. Geol.,* **85,** 289–300.

Lambeck, K., 1980. The Earth's Variable Rotation-Geophysical causes and consequences, Cambridge University Press, Cambridge.

Laskar, J., 1986. Secular terms of classical planetary theories using the results of general theory, *Astr. Astrophys.,* **157,** 59–70.

Laskar, J., 1988. Secular evolution of the Solar System over 10 millions years, *Astr. Astrophys.,* **198,** 341–362.

Laskar, J., 1990. The chaotic motion of the Solar System: a numerical estimate of the size of the chaotic zones, *Icarus,* **88,** 266–291.

Laskar, J., 1993. Frequency analysis of a dynamical system, *Celest. Mech.,* **61,** 191–196.

Laskar, J., 1999. The limits of Earth orbital calculations for geological time-scale use, *Phil. Trans. R. Soc. Lond.,* A, **357,** 1735–1759.

Laskar, J. & Robutel, P., 1993. The chaotic obliquities of the planets, *Nature,* **361,** 608–612.

Laskar, J., Joutel, F. & Boudin, F., 1993. Orbital, precessional, and insolation quantities for the Earth from −20 Ma to +10 Ma, *Astr. Astrophys.,* **270,** 522–533.

Lourens, L.J. & Hilgen, F.J., 1997. Long-period variations in the Earth's obliquity and their relation to third-order eustatic cycles and Neogene glaciations, *Quat. Int.,* **40,** 43–52.

Lourens, L.J., Antonarakou, A., Hilgen, F.J., Van Hoof, A.A., Vergnaud-Grazzini, A.M. & Zachariasse, W.J., 1996. Evaluation of the Plio-Pleistocene astronomical time scale, *Paleoceanography,* **11,** 391–413.

Maynard, J.R. & Leeder, M.R., 1992. On the periodicity and magnitude of Late Carboniferous glacio-eustatic sea-level changes, *J. geol. Soc. Lond.,* **149,** 303–311.

McCausland, P.J.A. & Hodych, J.P., 1998. Paleomagnetism of the 550 Ma skinner Cove volcanics of western Newfoundland and the opening of the Iapetus Ocean, *Earth planet. Sci. Lett.,* **163,** 15–29.

Meert, J.G., 2001. Growing Gondwana and rethinking Rodinia: A paleomagnetic perspective, *Gondwana Research,* **4,** 541–550.

Meert, J.G. & Van der Voo, R., 1994. The Neoproterozoic (1000–540 Ma) glacial intervals: No more Snowball Earth?, *Earth planet. Sci. Lett.,* **123,** 1–13.

Milankovitch, M., 1941. Kanon der Erdbestrahlung und seine Anwendung auf das Eiszeitproblem, *Akad. R. Serbe.,* **133,** 1–633, 1941. English translation, Canon of Isolation and the Ice Age Problem, *Alven Global*, 1998.

Mitrovica, J.X. & Forte, A.M., 1995. Pleistocene glaciation and the Earth's precession constant, *Geophys. J. Int.,* **121,** 21–32.

Mitrovica, J.X. & Peltier, W.R., 1993. The inference of mantle viscosity from an inversion of the Fennoscandian relaxation spectrum, *Geophys. J. Int.,* **114,** 45–62.

Mitrovica, J.X., Forte, A.M. & Pan, R., 1997. Glaciation-induced variations in the Earth's precession frequency, obliquity and insolation over the last 2.6 Ma, *Geophys. J. Int.,* **128,** 270–284.

Mix, A.C., Pisias, N.G., Rugh, W., Wilson, J., Morey, A. & Hagelberg, T., 1995. Benthic foraminiferal stable isotope record form Site 849, 0–5 Ma: Local and global climate changes, in *Proc. ODP, Sci. Results,* Vol. 138, pp. 371–512, eds Pisias, N.G., Mayer, L., Janecek, T., Palmer-Julson, A. & VanAndel, T.H., College Station, TX (Ocean Drilling Program).

Nakada, M. & Lambeck, K., 1989. Late Pleistocene and Holocene sea-level change in the Australian region and the mantle rheology, *Geophys. J. Int.,* **96,** 497–517.

Néron de Surgy, O. & Laskar, J., 1997. On the long term evolution of the spin of the Earth, *Astr. Astrophys.,* **318,** 975–989.

Pais, M.A., Le Mouël, J.L., Lambeck, K. & Poirier, J.P., 1999. Late Precambrian paradoxical glaciation and obliquity of the Earth -a discussion of dynamical constraints, *Earth planet. Sci. Lett.,* **174,** 155–171.

Paillard, D., 1998. The timing of Pleistocene glaciations from a simple multiple-state climate model, *Nature,* **391,** 378–381.

Park, J.K., 1997. Palaeomagnetic evidence for low-latitude glaciation during deposition of the Neoproterozoic Rapitan Group, MacKenzie Moutain, N.W.T Canada, *Can. J. Earth. Sci.,* **34,** 34–49.

Peltier, W.R., 1974. The impulse response of a Maxwell Earth, *Rev. Geophys.,* **12,** 649–669.

Peltier, W.R., 1985. The LAGEOS constraint on deep mantle viscosity: results from a new normal mode method for the inversion of viscoelastic relaxation spectra, *J. geophys. Res.,* **90,** 9411–9421.

Peltier, W.R., 1989. Global sea level and Earth rotation, *Science,* **240,** 895–901.

Peltier, W.R., 1994. Ice age paleotopography, *Science,* **265,** 195–201.

Raymo, M.E., Ruddiman, W.F., Backman, J. & Martinson, D.G., 1989. Late Pleistocene variation in northern hemisphere ice sheets and North Atlantic Deep Water Circulation, *Paleoceanography,* **4,** 413–446.

Roberts, J.D., 1976. Late Precambrian dolomites, Vendian glaciation and synchroneity of Vendian glaciations, *J. Geol.,* **84,** 47–63.

Rochester, M.G. & Smylie, D.E., 1974. On changes in the trace of the Earth's inertial tensor, *J. geophys. Res.,* **79,** 4948–4951.

Ross, C.A. & Ross, J.R.P., 1985. Late Paleozoic depositional sequences are synchronous and worldwide, *Geology,* **13,** 194–197.
Rubincam, D.P., 1990. Mars: Change in axial tilt due to climate?, *Science,* **248,** 720–721.
Rubincam, D.P., 1993. The obliquity of Mars and 'climate friction', *J. geophys. Res.,* **98,** 10 827–10 832.
Rubincam, D.P., 1995. Has climate changed Earth's tilt?, *Paleoceanography,* **10,** 365–372.
Rubincam, D.P., 1999. Mars secular obliquity change due to water ice caps, *J. geophys. Res.,* **104,** 30 765–30 774.
Ruddiman, W.F., Raymo, M.E., Martinson, D.G., Clement B.M. & Backman, J., 1989. Pleistocene evolution: northern hemisphere ice sheets and North Atlantic ocean, *Paleoceanography,* **4,** 353–412.
Schmidt, P.W. & Williams, G.E., 1995. The Neoproterozoic climatic paradox: Equatorial palaeolatitude for Marinoan glaciations near sea level in South Australia, *Earth planet. Sci. Lett.,* **134,** 107–121.
Shackleton, N.J., 1967. Oxygen isotope analysis and Pleistocene temperatures re-assessed, *Nature,* **215,** 15–17.
Shackleton, N.J., 2000. The 100 000 year ice–age cycle identified and found to lag temperature, carbone dioxide and orbital eccentricity, *Science,* **289,** 1897–1902.
Shackleton, N.J., Berger, A. & Peltier, W.R., 1990. An alternative astronomical calibration of the lower Pleistocene timescale based on ODP Site 677, *Phil. Trans. R. Soc. Lond.,* A, **81,** 251–261.
Shackleton, N.J., Crowhurst, S., Hagelberg, T., Pisias, N.G. & Schneider, D.A., 1995a. A new late Neogene time scale: Application to leg 138 Sites, in *Proc. ODP, Sci. Results*, Vol. 138, pp. 73–101, eds Pisias, N.G., Mayer, L.A., Janecek, T.R., Palmer-Julson, A. & Van Andel, T.H., College Station, TX (Ocean Drilling Program).
Shackleton, N.J., Hall, M.A. & Pate, D., 1995b. Pliocene stable statigraphy of ODP Site 846, in *Proc. ODP, Sci. Results*, . Vol. 138, pp. 337–353, eds Pisias, N.G., Mayer, L.A., Janecek, T.R., Palmer-Julson, A. & Van Andel, T.H., College Station, TX (Ocean Drilling Program).
Sohl, L.E., Christie-Blick, N.J. & Kent, D.V., 1999. Palaeomagnetic polarity reversals in Marinoan (ca 600 Ma) glacial deposits of Australia: Implications for the duration of low-latitude glaciation in Neoproterozoic time, *Geol. Soc. Am. Bull.,* **111,** 1120–1139.
Spada, G. & Alphonsi, L., 1998. Obliquity variations due to climate friction on Mars: Darwin versus layered models, *J. geophys. Res.,* **103,** 28 599–28 605.
Thomson, D.J., 1990. Quadratic inverse spectrum estimates: Application to paleoclimatology, *Phil. Trans. R. Soc. Lond.,* A, **132,** 539–551.
Tiedemann, R., Sarnthein, M. & Shackleton, N.J., 1994. An astronomical time scale for the Pliocene Atlantic δ^{18}O and dust flux records of ODP Site 659, *Paleoceanography,* **9,** 619–638.
Torsvik, T.H., Smethurst, M.A., Meert, J.G., Van der Voo, R., McKerrow, W.S., Brasier, M.D., Sturt, B.A. & Walderhaug, H.J., 1996. Continental break-up and collision in the Neoproterozoic and Palaeozoic-a tale of Baltica and Laurentia, *Earth Sci. Rev.,* **40,** 229–258.
Tushingham, A.M. & Peltier, W.R., 1991. ICE-3G: A new global model of Late Pleistocene deglaciation based upon geophysical predictions of post-glacial relative sea-level change, *J. geophys. Res.,* **96,** 4497–4523.
Veevers, J.J, Powell, C., McA, Collinson, J.W. & Lopez-Gamundi, O.R., 1994. Permian-Triassic Pangea basins and foldbelts along the Panthalassan margin of Gwondanaland, *Geol. Soc. Am. Memoir,* Vol. 184, pp. 331–353, eds Veevers, J.J. & Powell, C., McA.
Weil, A.B., Van Der Voo, R., Niocaill, C.M. & Meert J.G., 1998. The Proterozoic supercontinent Rodinia: paleaomagnetically derived reconstructions for 1100 to 800 Ma, *Earth planet. Sci. Lett.,* **154,** 13–24.
Williams, G.E., 1975. Late Precambrian glacial climate and the Earth's obliquity, *Geol. Mag.*, *112,* 441–465.
Williams, G.E., 1993. History of the Earth's obliquity, *Earth Sci. Rev.,* **34,** 1–45.
Williams, D.M., Kasting, J.F. & Frakes, L.A., 1998. Low-latitude glaciations and rapid changes in the Earth's obliquity explained by obliquity–oblateness feedback, *Nature,* **396,** 453–455.
Wu, P. & Peltier, W.R, 1984. Pleistocene deglaciation and the Earth's rotation: a new analysis, *Geophys. J. R. astr. Soc.,* **876,** 753–791.

APPENDIX A: LONG-TERM DYNAMICAL EVOLUTION

Here, we analyse the dynamic equations obtained in the previous sections. The main purpose is to search the equilibrium points of the obliquity for the climate friction effect corresponding to a cancellation of the secular obliquity change. This provides information about some long-term scenarios of the obliquity evolution in case of uninterrupted ice-ages with glacial cycles, in the same spirit as the work of Correia *et al.* (2003), and Correia & Laskar (2003) on tidal friction and core–mantle friction. The mean obliquity $\bar{\varepsilon}$ is now assimilated to the obliquity ε. For the dominant obliquity cycle and a constant oblateness change, the secular obliquity change is rewritten from (14) and (48) as

$$\frac{d\varepsilon}{dt} = K\Theta_1 \frac{\alpha\cos\varepsilon}{\alpha\cos\varepsilon + s_3}(\sin\zeta_i - f(\zeta_s)\sin(\zeta_i + \zeta_s)) \tag{A1}$$

where K is a positive constant and $\alpha\cos\varepsilon + s_3 = \nu_1$ the main obliquity-cycle frequency. Phase lag parameters ζ_i and ζ_s are functions of ν_1 and hence of the obliquity value. We used here the function $\zeta_s(\nu_1)$ given in Section 3 corresponding to the viscoelastic model B. ζ_s is thus an increasing function of the obliquity frequency and a decreasing function of the obliquity. The dependence of the ice sheet phase to obliquity frequency forcing is less constrained. Here, we adopt a simple linear model and assume that the response time delay T_i is independent of the obliquity frequency forcing. In that case, the phase lag $\zeta_i = \nu_1 T_i$ is proportional to ν_1 and is also a decreasing function of the obliquity, as in the Imbrie and Imbrie model. We additionally consider that the ice sheet response time lag T_i could not realistically be longer than the obliquity period, leading to the condition $\zeta_i < 360^\circ$. With the previous assumptions, the secular obliquity change (A1) is rewritten as

$$\frac{d\varepsilon}{dt} = K\Theta_1 \frac{\alpha\cos\varepsilon}{\alpha\cos\varepsilon + s_3} H(\varepsilon, T_i) \tag{A2}$$

where

$$H(\varepsilon, T_i) = \sin(\nu_1(\varepsilon)T_i) - f(\zeta_s(\varepsilon))(\sin(\nu_1(\varepsilon)T_i + \zeta_s(\varepsilon)) \tag{A3}$$

Eq. (A1) becomes infinite for the spin-orbital resonance $\nu_1 = \alpha\cos\varepsilon + s_3 = 0$ which corresponds to an obliquity close to 71° for the present precession constant $\alpha_0 \simeq 54.93''/\text{yr}$. In any case, the linear theory cannot be used close to spin-orbital resonances and thereby in the ∼60–90° chaotic obliquity zone (Laskar *et al.* 1993).

The equilibrium obliquities ε_e are obtained for $d\varepsilon/dt = 0$. A first value is obtained from (A2) for $\varepsilon_e = 90^\circ$ ($\cos\varepsilon_e = 0$). Other equilibrium points are given by $H(\varepsilon_e, T_i) = 0$ when the secular obliquity change induced by the ice sheet response is strictly compensated by the opposite Earth's deformation effect. For $\varepsilon < 90^\circ$, these equilibrium points are stable if

$$\frac{\partial H(\varepsilon, T_i)}{\partial\varepsilon}(\varepsilon_e, T_i) < 0. \tag{A4}$$

The extreme values $\varepsilon = 0^\circ$ and $\varepsilon = 180^\circ$ are not equilibrium obliquities which are apparent solutions of (A2). For these values, the precession angle ψ is not defined. These singularities can be eliminated by replacing ψ and ε by the complex variables $\Psi = \sin\varepsilon \times e^{i\psi}$ and $X = \cos\varepsilon$. The precession eqs (1) then become:

$$\begin{aligned}\dot{X} &= -Re\,[(\mathcal{A}(t) + i\mathcal{B}(t))\Psi] \\ \dot{\Psi} &= i[\alpha X - 2\mathcal{C}(t)]\Psi + X\,[\mathcal{A}(t) - i\mathcal{B}(t)]\,.\end{aligned} \tag{A5}$$

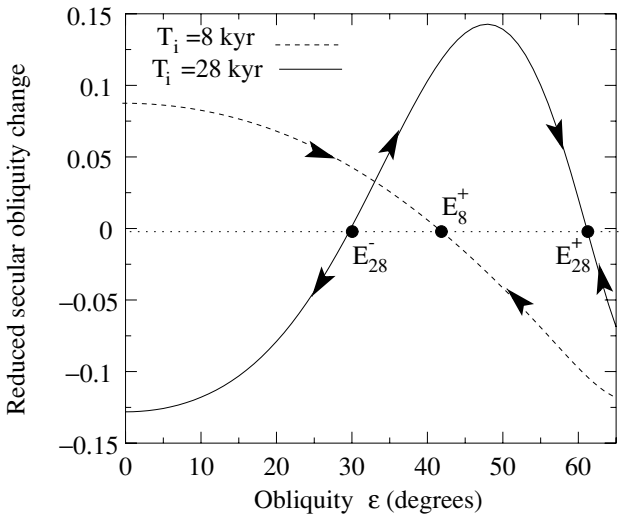

Figure A1. The function $H(\varepsilon, T_i)$ as a function of the obliquity for two different constant values of T_i. The intersection with the x-axis gives the equilibrium obliquities and the direction of the arrows indicates the trajectories around the fixed points. E_{28}^- is the unstable equilibrium obliquity for $T_i = 28$ kyr, E_8^+ and E_{28}^+ are the respective stable equilibrium obliquities for $T_i = 8$ kyr and 28 kyr.

For small obliquities, we have $\dot{\Psi}|_{\Psi=0} = X\,[\mathcal{A}(t) - i\mathcal{B}(t)]$. The precession motion is then forced by the planetary perturbations which induce a residual forced obliquity, preventing the possibility of an obliquity–oblateness feedback. The function $H(\varepsilon, T_i)$ is plotted in Fig. A1 for different values of T_i and $\alpha = \alpha_0$. For the current value T_i= 8 kyr and for the present obliquity, we retrieve a positive secular obliquity change and the local negative slope for the critical point $\varepsilon_e \simeq 42^\circ$ corresponds to a stable equilibrium point. For the time lag $T_i = 28$ kyr, there is one stable equilibrium point $\varepsilon_e \simeq 60^\circ$ while the other fixed point $\varepsilon_e \simeq 30^\circ$ is unstable. A systematic numerical search of equilibrium states of obliquity and of their stability is summarized in the bifurcation diagram of the Fig. A2. A pitchfork bifurcation structure is exhibited with two stable branches and one

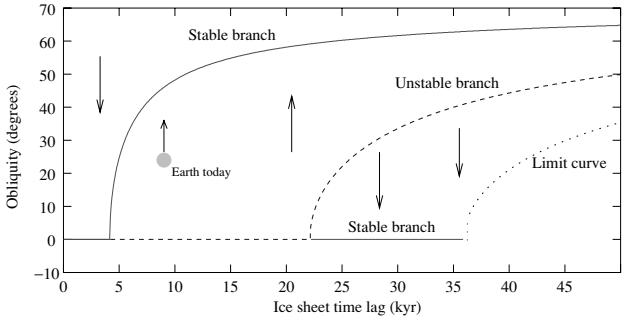

Figure A2. Equilibrium points of the Earth's obliquity for the climate friction effect as a function of the ice sheet time lag T_i. The stable branches (solid line) correspond to stable equilibrium states of the obliquity. For a given initial obliquity and a constant value of T_i, the obliquity follows a vertical line towards the attractive stable branch and escaping to the unstable branch (dashed line). An example is provided with the present initial conditions ($\varepsilon_0 = 23.44^\circ$, $T_i = 8$ kyr) corresponding to a positive obliquity drift. The points at the right of the limit curve (dotted line) correspond to unrealistic ice time lags higher than the obliquity period (or $\zeta_i > 2\pi$).

unstable branch. The stable branches correspond to stable and attractive equilibrium obliquities. For the current value $T_i = 8$ kyr, climate friction drives the Earth to an equilibrium state close to 42°. However, we stress that with a current $\sim$0.01 deg Myr^{-1} rate, it would take 1 Gyr of steady glaciations to obtain an obliquity change of only 10°. For most acceptable values of the ice time lag and of initial obliquities, the secular obliquity change is positive and drives the obliquity to an equilibrium point different from 90°. Only for very low (<4.2 kyr) and large (>22.1 kyr) time lag values, the climate friction effect is dominated by the viscous dissipation which tends to bring the spin to 0°. We considered here that the oblateness change was independent of the obliquity. Higher obliquity implies probably smaller polar ice caps and hence smaller change of oblateness. It then may exist high obliquity values, for which the ice is not concentrated at any latitudes, and continental configurations which cancel the change of oblateness, adding additional equilibrium points to the bifurcation diagram.